Annu. Rev. Astron. Astrophys. 1992. 30: 457–98

LONG-BASELINE OPTICAL AND INFRARED STELLAR INTERFEROMETRY

M. Shao and M. M. Colavita

Optical Sciences and Applications Section, Jet Propulsion Laboratory, California Institute of Technology, 4800 Oak Grove Dr., Pasadena, California 91109

KEY WORDS: astrometry, high resolution imaging, adaptive optics

1. INTRODUCTION

The field of modern long-baseline optical[1] stellar interferometry has made enormous strides since the first independent-element Michelson stellar interferometer in 1974. Presently, several interferometers are operating on a continuous basis, demonstrating that the technical problems that plagued the advance of direct interferometry for so many decades after Michelson's pioneering experiments have been solved. More than mere technology demonstrations, these current instruments, with their high angular resolution, have generated significant scientific results. While optical interferometry, with its greater technical challenges, has lagged behind its radio counterpart, the next generation of ground-based interferometers are poised to exploit some of the key concepts of modern radio interferometry, especially the use of closure phase among independent telescopes. Interferometry in space is also seeing a maturation of concepts, drawing upon the experience of ground-based instruments, and several detailed instrument designs have been proposed for future space missions. In addition, concepts have been proposed for second-generation space and lunar interferometers, showing the scientific potential of such future instruments. However, in the near term, the most interesting scientific prospects are

[1] Throughout the text, optical refers to both visible and infrared wavelengths.

0066–4146/92/0915–0457$02.00

from the next generation ground-based and the first-generation space-based stellar interferometers.

2. INTERFEROMETRY ON THE GROUND

2.1 *Past and Current Instruments*

The use of interferometry to extract science information from observations of celestial sources dates back to Fizeau (50), who noted that the diameter of an extended disk could be determined interferometrically from measurement of the baseline length at which the fringe contrast dropped to zero. This concept was exploited by Michelson & Pease (104, 105) in 1920 in observations using the 100″ Hooker telescope at Mt. Wilson. Using mirrors spaced by up to 6.1 m mounted to a beam on the top of the telescope tube, and using the 100″ telescope as a pointer and beam combiner, they ultimately measured the diameter of six supergiant stars with sizes between 20 and 47 mas (milliarcsec). In doing so they made the important observation that despite the motion of the interference fringes, the fringe contrast remained high, i.e. that high angular resolution information could be extracted from short exposures despite the presence of atmospheric turbulence. Subsequent to the experiments on the 100″ telescope, a dedicated stellar interferometer was built on Mt. Wilson (120, 121). However, the technology of the day was inadequate to allow successful operation of this instrument.

The next major long-baseline optical interferometric instrument was the Intensity Interferometer, which operated at Narrabri, Australia from 1963 to 1972 (62–64), following the demonstration in 1956 of optical intensity interferometry by Hanbury Brown & Twiss (65). An intensity interferometer correlates the detected irradiance from two spatially-separate apertures in order to obtain the fringe amplitude. The Intensity Interferometer at Narrabri used 6.5 m diameter incoherent light collectors over baselines of 10–150 m, and measured the diameter of 32 stars visible from its southern-hemisphere site. These stars ranged in diameter from 0.44–5.10 mas, and were brighter than 2.5 mag. While the Narrabri instrument was very successful, the extension of intensity interferometry to fainter objects is limited by the low sensitivity of the technique; in addition, the technique is incapable of measuring the fringe phase, which is essential for true imaging.

Modern long-baseline optical Michelson interferometry probably begins with the interferometer of Labeyrie (82) in 1974. His instrument was a true Michelson interferometer, and was the first to obtain direct interference fringes between separate telescopes, over an initial baseline of 12 m. To maintain equal pathlengths in the two interfering beams, Labeyrie used a

beam-combiner table which moved at the sidereal rate, and observed the fringes visually and with a TV camera. This instrument, the I2T (Interféromètre à Deux Télescopes), was upgraded over time to include a longer, variable baseline and more sophisticated electronics (75), and has made a number of high-resolution observations (43, 60, 76, 77). Presently the I2T is being upgraded to the I3T (CHARON), to include active fringe tracking as well as a third telescope (138).

The Mark I stellar interferometer by Shao and Staelin in 1979 (153, 154) was the first stellar interferometer to demonstrate photoelectric fringe detection and phase-coherent fringe tracking. The Mark I was succeeded by the Mark II (151) from 1982–1984, and by the Mark III interferometer (150) in 1986, which is presently operating on Mt. Wilson. Scientific results from the Mark III include wide-angle astrometric measurements (107, 147), the determination of stellar diameters (70, 109, 149), studies of binary stars (117, 118), and measurements of atmospheric propagation (32, 33). The Mark III will be discussed in more detail below.

While there are important sensitivity advantages to Michelson interferometry in the visible and infrared, heterodyne methods can be used at mid-infrared wavelengths. After heterodyning to an intermediate frequency, the signal processing is identical to that of a radio interferometer (172). In 1974, Johnson et al (72) constructed a heterodyne interferometer using the two 81 cm McMath auxiliary telescopes at Kitt Peak. This instrument had a 5.5 m baseline and used a CO_2-laser local oscillator. It measured the phase and amplitude of the 11.106 μm infrared radiation, and observed the spatial distribution and the positions of several bright infrared sources (160–163). In 1988, Townes and coworkers (17, 38) began operation of a dedicated Infrared Spatial heterodyne Interferometer (ISI), presently located on Mt. Wilson. This instrument uses two 1.65 m aperture telescopes which can be positioned to yield variable baseline orientations. Initial scientific results include the study of dust shells (16, 37) and atmospheric propagation (15).

Based on the success of these instruments, and on advancing technology in controlled optics, detectors, and automation, there is presently much activity in the interferometry field. Other interferometer projects which have demonstrated at least initial operation include: the GI2T (Grand Interféromètre à Deux Télescopes) (86, 106) at CERGA, France—a successor to the I2T, using two 1.5 m spherical-mount telescopes, with baselines initially to 70 m, and using multi-r_0 beam combination; the SUSI (Sydney Univ. Spatial Interferometer) prototype (41, 42) at Sydney, Australia—an 11.4-m prototype for the much longer baseline SUSI (discussed later); SOIRDETE (Synthèse d'Overture en InfraRouge à Deux Télescopes) (56) at CERGA—an infrared interferometer using a fixed

15 m baseline with two 1 m telescopes and drift-scanning of the interference fringes; IRMA (Infrared Michelson Array) (44, 45) in Wyoming—a near-infrared interferometer with baselines from 2.5–19.5 m, also using drift-scanning; and COAST (Cambridge Optical Aperture Synthesis Telescope) (95) at Cambridge, UK—a visible/near-infrared interferometer with baselines to 100 m. In addition, a number of ambitious projects are planned, some of which will be discussed below. Several recent conference proceedings provide useful compilations of activity in the field (9a, 22, 102); (59) provides an extensive bibliography of ground and space interferometry.

2.2 *Michelson Interferometry*

In its fundamentals, optical interferometry differs little from radio interferometry. In particular, both techniques image synthetically through observation of an object's complex fringe visibility, or mutual coherence function, at various baseline lengths and orientations. These observations are related to the object's irradiance distribution through the van Cittert-Zernike theorem (18, 170), which gives the irradiance distribution as a Fourier transform of the complex visibility measurements. Let $\Gamma(u,v)$ be the complex fringe visibility $Ve^{i\phi}$, where V and ϕ are the fringe amplitude and phase. The Fourier plane coordinates are given by the projected baseline vector, i.e. $(u,v) = \bar{\mathbf{B}}_p/\lambda$, where $\bar{\mathbf{B}}_p$ is the projected baseline vector perpendicular to the direction of the source and λ is wavelength. The (normalized) source irradiance $I(x,y)$, in angular coordinates, is related to its complex visibility as (119)

$$\Gamma(u,v) = \iint I(x,y)\exp\left[-2\pi i(ux+vy)\right]dx\,dy. \qquad 1.$$

Given a maximum projected baseline length B_{max}, an interferometer samples spatial frequencies out to B_{max}/λ, and thus the angular resolution of an interferometer is essentially the same as that of a filled-aperture telescope with a diameter equal to the maximum baseline. In practice, an inverse transform is never used to retrieve the source distribution; rather, powerful inversion algorithms have been developed in radio astronomy to transform uncalibrated visibility measurements to the object irradiance (119). It is important to note that full sampling of the u–v plane is not necessary: of order as many u–v points need be sampled as there are object points. In addition, while the fringe phase ϕ is necessary for true imaging, measurements of just the fringe amplitude can be used for parametric imaging of simple objects—disks, dust shells, binary stars, etc—as is done with the current generation of ground-based instruments.

For astrometry, both radio and optical interferometers exploit the relation between the measured fringe position, or delay, d, and the source position (151, 170):

$$d = \bar{\mathbf{B}} \cdot \hat{\mathbf{s}} + C, \qquad 2.$$

where $\bar{\mathbf{B}}$ is the baseline vector, $\hat{\mathbf{s}}$ is the source unit vector, and C is the delay off-set, an instrument-dependent constant. Observations of multiple sources allow for determination of both source positions and instrument parameters.

Figure 1 shows a schematic of a simple two-element Michelson interferometer (cf 167). Light is collected by two apertures, typically siderostats or telescopes, and is routed to a combining beamsplitter. A variable optical path delay is inserted into one, or both arms, using delay lines or a moving beam combiner, in order to match the path delays from the incident wavefront to the beamsplitter via each arm of the interferometer. If these pathlengths are matched to within a few wavelengths, an interference fringe is detected. The complex fringe visibility is the phase and amplitude of the interference pattern. The delay is the measured delay-line position

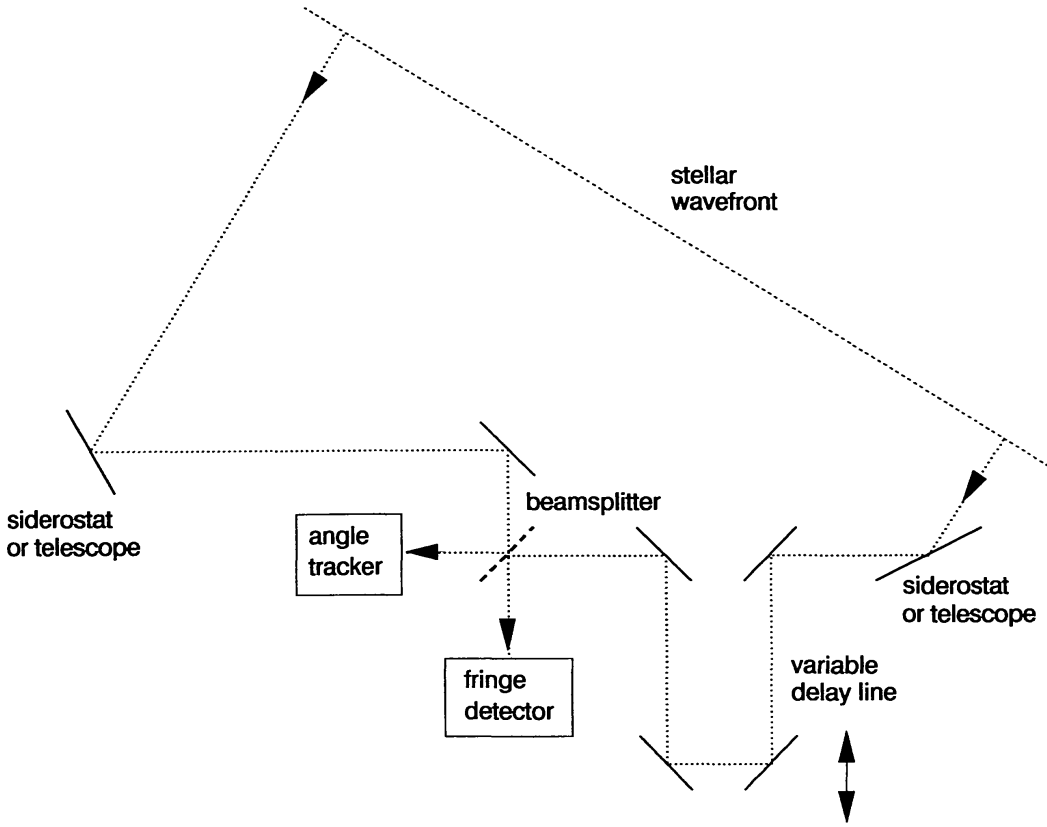

Figure 1 Schematic of a Michelson stellar interferometer.

at which the fringe is detected. Analogous to the pointing of the individual antennas in a radio array, the beams from the two interferometer apertures must be coalinged to better than the diffraction limit of the subapertures.

Clearly, a significant difference between optical and radio interferometry is wavelength. For one, instruments operating at the shorter optical wavelengths are far more sensitive to linear errors in pathlength and baseline orientation. For another, the noise properties at optical wavelengths are quite different from those at radio wavelengths. To obtain high sensitivity requires direct (Michelson) techniques, in which phase delays and interference are performed at optical wavelengths, as in Figure 1. For a direct-detection interferometer, the dominant noise source is photon shot noise from the source at visible wavelengths, or from the background at infrared wavelengths. For a heterodyne interferometer, the dominant noise source is photon shot noise from the local oscillator, leading to a noise of one photon per Hz of bandwidth [equivalently, a receiver noise temperature of $h\nu/k$, the quantum limit (158, 170)]. For short wavelengths, these noise characteristics strongly favor direct detection. In addition, the usable bandwidths are quite different between the two techniques, e.g. a 20% bandwidth at visible wavelengths is 100 THz, a (technologically) impractical bandwidth to process using heterodyne techniques. While the advantages of direct detection are extremely large at visible wavelengths, heterodyne techniques can be used in the mid-infrared, and have certain advantages (172), although they still suffer from a sensitivity penalty. An additional distinction between optical and radio interferometry is the absence, for fundamental reasons, of low noise amplifiers at optical frequencies: Any amplifier must have a noise temperature of at least $h\nu/k$. Thus signal division among the various baselines in a multi-element interferometer is not without a noise penalty. Aspects of signal-to-noise ratio in multi-element optical interferometers are discussed in detail by Prasad & Kulkarni (122) and Kulkarni et al (80).

Another major difference between optical and radio interferometry is the significant impact of clear-air turbulence on optical propagation. While the linear optical pathlength fluctuations at optical and radio wavelengths due to turbulence are roughly comparable, the much shorter wavelengths in the optical lead to qualitatively different results. This topic is well discussed in several reviews and books (71, 89, 130, 159, 167) and references therein. For interferometry, the major effect of turbulence is the imposition of random phase delays on the incident radiation. These phase fluctuations limit both the transverse coherence length of the incident stellar radiation, as well as the coherence time of the interference pattern. Transverse coherence diameter is described by the Fried length r_0 (52), which is that diameter aperture over which the phase fluctuations are approximately one radian

rms; coherence time is described by the parameter τ_0 (cf 167), which is that time interval during which the fluctuations in the phase of the fringe pattern are one radian rms—essentially, the time for the wind to translate the turbulence by r_0. A Michelson interferometer, which measures coherence, must operate coherently, and to first order is thus constrained to use subapertures smaller than r_0, and coherent integration times smaller than τ_0. Thus, like speckle interferometry (36, 81), short exposures are required in order to extract high resolution information. At visible wavelengths, and with typical 1″ seeing, the coherence diameter and coherence time are $\sim$10 cm and $\sim$10 ms. However, both r_0 and τ_0 scale with wavelength as $\lambda^{6/5}$, so that larger apertures and coherence times are usable at longer wavelengths: $\sim$3 m and 0.3 s at 10 μm with 1″ seeing, for example. In single-r_0 mode, visible-wavelength observations are typically limited to $\sim$10 mag. Advanced techniques to increase sensitivity are discussed below.

In addition to the sensitivity limits imposed by the atmosphere, there are also fundamental imaging constraints imposed. In particular, the atmospheric phase fluctuations, which can be many cycles in extent, severely corrupt the measured fringe phase. This effect, in addition to the limited u–v coverage of present-generation instruments, limits imaging with present instruments to phaseless parametric modeling of relatively simple sources: disks, shells, binary stars, etc. However, the high angular resolution achievable with interferometric techniques gives high value to these observations. Closure-phase techniques are required for true imaging, and will be discussed below. Finally, the large spatial scales associated with turbulence also limit the astrometric accuracy of an interferometer. In spite of this, the ability to accurately calibrate the instrumental errors of an interferometer, as well as the ability to apply two-color techniques to reduce atmospheric errors (33), allow extremely accurate astrometry despite the atmosphere.

2.3 *The Mark III Stellar Interferometer*

To show the current state of ground-based Michelson stellar interferometry, this section gives a brief description of the Mark III stellar interferometer, as well as a discussion of data processing and some scientific results in the areas of astrometry, stellar diameters, and binary stars.

INSTRUMENT AND OPERATIONAL DESCRIPTION The Mark III stellar interferometer (150) is the third in a series of interferometers constructed at Mt. Wilson, California. It succeeds the Mark I (154) and Mark II (151) interferometers, which were technology prototypes. The Mark III interferometer was designed initially with the goal of precise wide-angle astrometry, and was later augmented to perform parametric imaging. The instru-

ment has been in nearly continuous operation since first fringes in 1986 with observers from several institutions.

A schematic of the present configuration of the Mark III is given in Figure 2. For astrometry, three fixed siderostats are used to provide two baselines, one 12 m N-S, and the other 12 m E-S. For imaging, two movable siderostats are used to provide a number of baselines between 3 and 31.5 m N-S. The three siderostats used for astrometry, where long-term baseline stability is important, are of a fairly massive design and are mounted on large concrete piers. They are housed in insulated shelters which are air conditioned during the day to the nighttime temperature (as is the beam combiner lab). The two siderostats used for imaging have a less massive mechanical design, and are movable among 11 fixed stations using a removable rail assembly. All siderostats use alt-az mounts with a fixed fold mirror to maintain proper image rotation. The effective aperture of the system is 7.5 cm, which is much smaller than the r_0 values at Mt. Wilson, which reach $\sim$30 cm at visible wavelengths during good seeing, but is also large enough so that diffraction effects are small (166) and reimaging optics are unnecessary.

The afocal beams from two of the five available siderostats are routed through vacuum pipes to the central beam combining laboratory. The vacuum pipes minimize the effects of ground seeing, but are primarily employed to minimize dispersion. With a white-light interferometer, it is necessary to match the thicknesses of dispersive materials in each arm in order to yield high contrast fringes; the air paths of the Mark III match to within $\sim$3 cm, and the thickness of the transmissive optics are matched to <25 μm. Except for vacuum windows, and the beamsplitter/compensator, the predetection optics are all reflective.

Inside the beam combiner lab, the light from two siderostats is directed to two guiding mirrors. These piezoelectrically driven mirrors adjust the tilts of the two beams so that they are parallel when they interfere; with subaperture diffraction of $\sim 2''$, the tolerance on parallelism is $\sim 0.1''$. After reflection from the tilt mirrors, the stellar beams are directed into two optical delay lines. These delay lines equalize the path delays from the incident wavefront to the beamsplitter via each interferometer arm. The delay lines are implemented as optical retroreflectors using a cat's-eye configuration, which returns a parallel, but displaced beam. The delay-line design is based upon that of Connes (35), which was originally developed for Fourier transform spectroscopy. The positions of the delay lines are measured with laser interferometers and controlled to $\sim$10 nm as required to avoid smearing of the fringe pattern. The two delay lines, each with a physical travel of 5 m, provide a total adjustable delay of 20 m of optical path. The delay lines are installed in vacuum tanks, again for control of

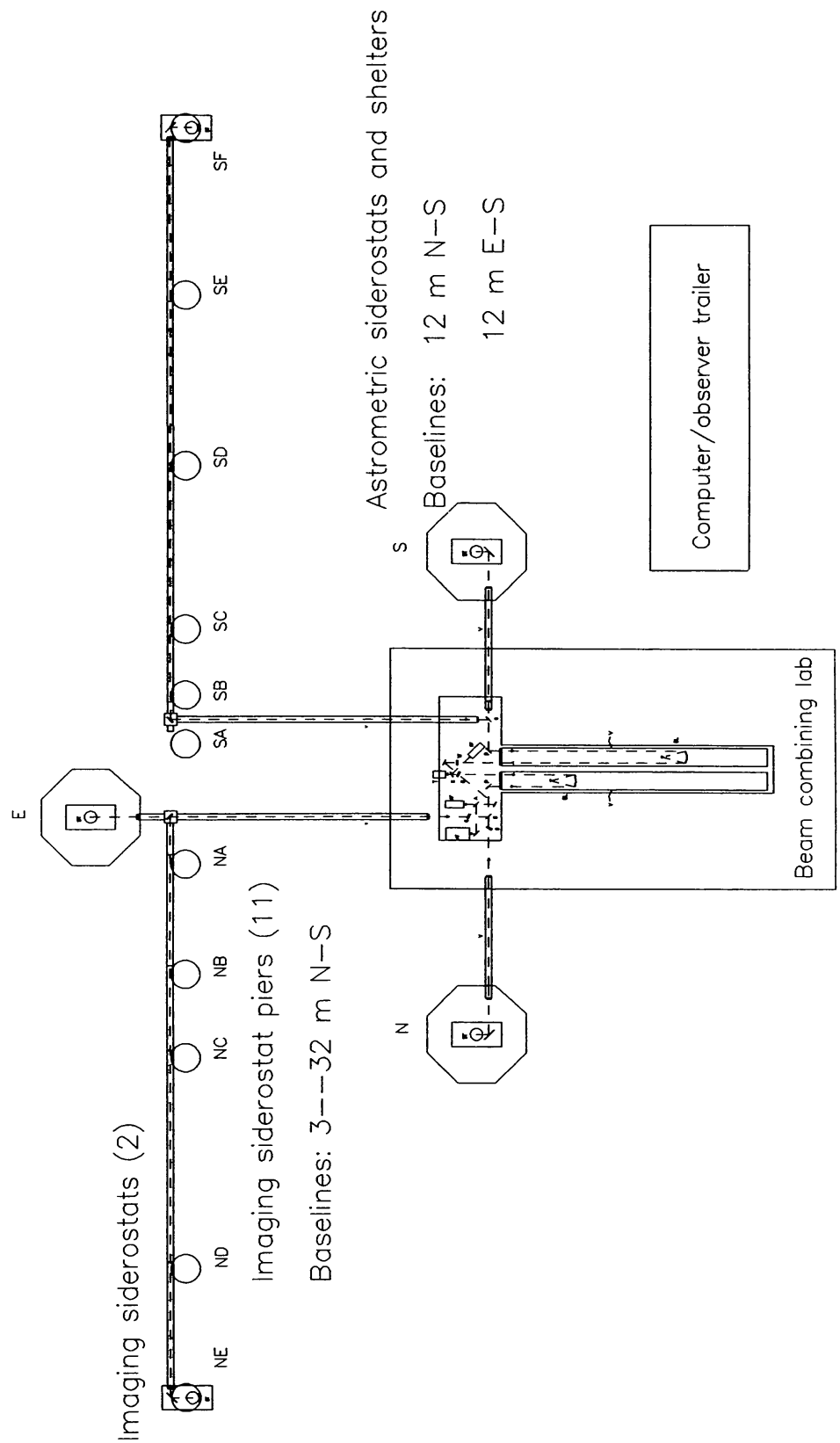

Figure 2 Schematic of the present configuration of the Mark III stellar interferometer on Mt. Wilson.

dispersion. With this implementation, first-order astronomical refraction is eliminated—a significant advantage for wide-angle astrometry.

After output from the delay lines, the light from the two apertures is interfered at a beamsplitter. The output from the two sides of the beamsplitter is directed to 4 photon-counting detectors via fiber optics: a wideband channel, from 0.55 to 1.0 μm for fringe tracking, and three narrowband channels, typically $\sim$20 nm wide and located between 450 and 800 nm, for precise amplitude measurements. To measure the phase and amplitude of the interference fringes, a 500 Hz triangular pathlength modulation is introduced into one arm of the interferometer. As the fringes are scanned across the detectors, photon counts in each channel are accumulated into four, $\lambda/4$-wide bins. These photon counts are coadded to a 4 ms coherent integration time ($\ll \tau_0$ at Mt. Wilson) and from the four bin counts for each channel, the total photon count N, as well as the X and Y quadratures are derived. From these the fringe phase and amplitude can be determined. The Mark III is an active interferometer, and the measured fringe phase on the wideband channel, where the SNR per 4 ms is $\gg 1$, is used to co-phase the interferometer by servoing the delay line position to track the white-light fringe. A closed-loop bandwidth of 20 Hz is used, which allows tracking to 1 rad rms under good seeing conditions [this bandwidth is independent of baseline (61)]. Using the inner 5 cm of the apertures (the annulus is used for angle tracking), an 8 ms coherent integration time, and light from one side of the beamsplitter, the Mark III achieves an active-mode limiting magnitude of $\sim$6 mag. All aspects of the Mark III, including fringe acquisition and tracking, star tracker acquisition and tracking, and data recording, are automated. On a night of good seeing, 150–200 90-sec observations are possible without significant operator intervention.

ASTROMETRY Astrometry with an optical interferometer (107, 147, 151) is very similar to VLBI astrometry, with the defining relation given by Equation 2. As astrometry is relative to the baseline vector, pains were taken with the Mark III to ensure its stability. In addition, in order to stabilize the delay constant, the optics for beam combination are mounted on an Invar breadboard. The resulting baseline stability is typically $\sim$1 μm per hour.

The fundamental astrometric observable is the fringe position, or delay, given by the sum of the laser-monitored delay-line position plus the fringe-tracker error. The observational strategy with the Mark III is to rapidly and repeatedly cycle through a list of target stars using a cycle time of $\sim$45 min. For measurements relative to the local centroid, rapid star switching chops out systematic instrumental effects and large spatial scale

atmospheric errors. Once per switching cycle, the delay constant C is calibrated by retroreflecting the siderostats, injecting a white light source, and measuring the delay at which the internal white-light fringe is detected. The astrometric reduction of data, given the delay measurements and constant calibrations, is described in detail in (147).

Even with an ideal interferometer, the accuracy of the astrometric positions will be limited by atmospheric turbulence. At visible wavelengths, two-color methods can be used to reduce the atmospheric error (33, 147, 153). To first order, with a dispersive atmosphere, random fringe-position displacements about the nominal zero (sidereal) position are systematically larger at shorter wavelengths. Thus, from measurement of the fringe positions at two widely-separated colors, and from knowledge of the value of the atmospheric dispersion, one can extrapolate the fringe position to the value it would have had in the absence of atmospheric turbulence. Thus, if d_R and d_B are the delays measured in red and blue channels, the corrected delay is given by $d_{2C} = d_R - D(d_B - d_R)$, where D is a dispersion measure: $D = n_R/(n_B - n_R)$, and n is refractive index. In practice, the two-color technique is limited by several error sources, the most important being water-vapor turbulence, which is the residual remaining after correction of the dominant temperature-driven turbulence. Despite these limitations, improvements in astrometric accuracy by factors of between 3 and 10 are possible for an instrument limited only by the atmosphere.

Figure 3 shows the results from a series of astrometric measurements made in 1988 (147). The set of 12 target stars spanned 7.0 hrs in RA, and 30° in dec, and were observed on the 12 m N-S and 12 m E-S astrometric baselines over 5 nights, for a total of 588 scans on the target stars. A consistent baseline for each night was determined from the a priori FK5 positions. The average formal errors for this data set were 9.2 and 5.6 mas in RA and dec, respectively, for a solution utilizing constant term calibration and two-color atmospheric correction. These values are significantly better than those achieved using conventional wide-angle astrometric instruments. Repeated measurements of this set of stars in 1989 yielded $\sim 60\%$ of the stars within the 1-σ error bars of the 1988 positions.

STELLAR DIAMETERS Traditionally, the measurement of stellar diameters has been the objective of long-baseline interferometry. The principles of stellar diameter measurement are well known (62): by the van Cittert-Zernike relation, the fringe visibility of an extended disk is given by the Airy formula

$$V = 2J_1(kB_p\theta/2)/(kB_p\theta/2), \qquad 3.$$

where B_p is the projected baseline length, θ is the stellar diameter, and k

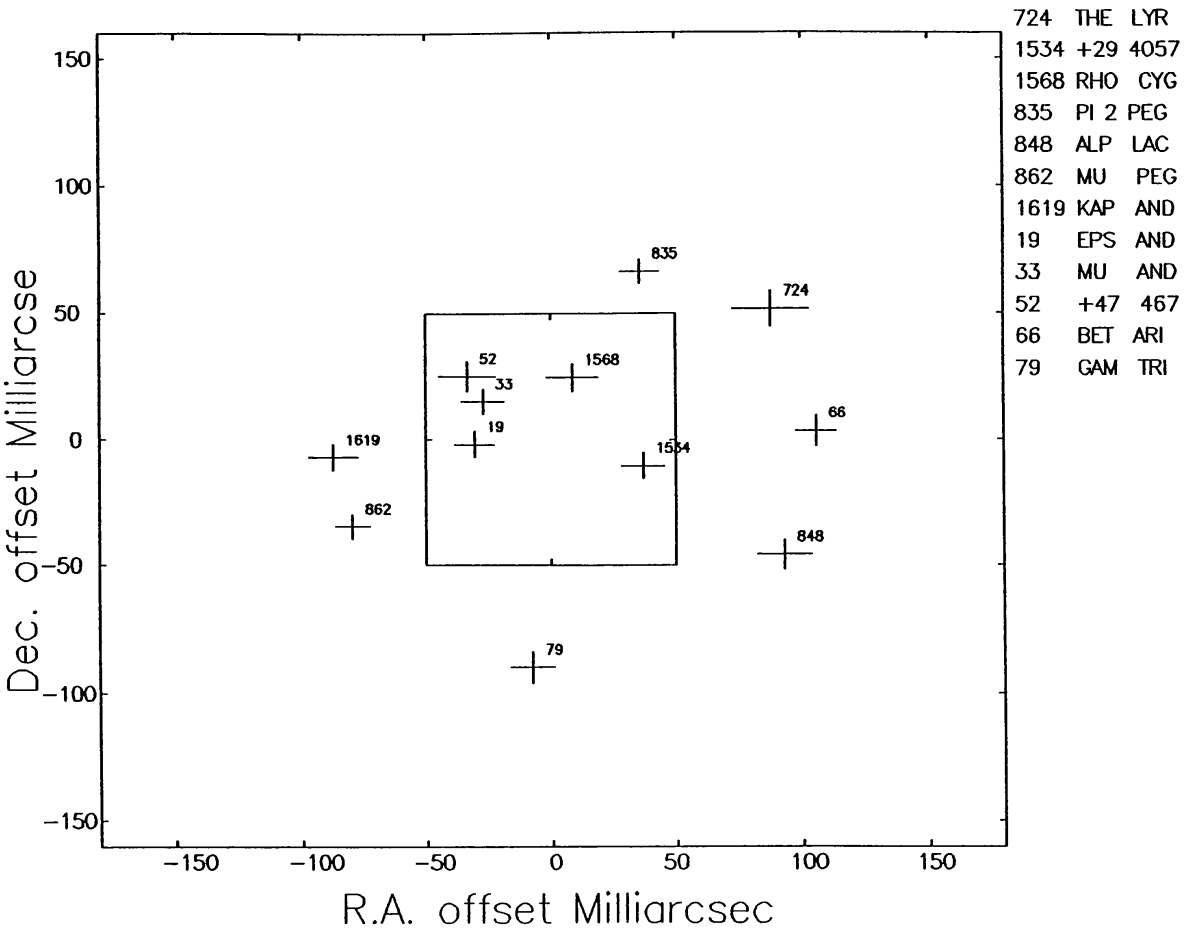

Figure 3 Wide-angle astrometric results with the Mark III from (148). The positions of the crosses are the offsets from the catalogued FK5 positions; the sizes of the crosses are the 1σ formal errors. The set of stars spanned 7.0 hrs in RA and 30° in dec.

is wavenumber $2\pi/\lambda$. Tyically, the star would be larger than $\sim\lambda/2B_p$, for which the intrinsic visibility is 72%. In principle, from measurements of visibility at different baseline lengths, one performs a nonlinear least-squares fit for the stellar diameter; it is not necessary to seek the visibility null.

In practice the process is similar, but somewhat more complex. For example, the preferred observable at optical wavelengths is squared visibility amplitude V^2, which can be estimated in an unbiased fashion in the presence of photon noise (70, 149, 167). However, when the objective is to obtain stellar diameters with precisions of order 1%, the most important practical consideration is calibration. As noted earlier, turbulence ordinarily limits operation of an active interferometer to subapertures $d < r_0$ and coherent integration times $\tau < \tau_0$. However, even when these constraints are obeyed, there still remain significant visibility biases due to the atmosphere. For $d = r_0$ and $\tau = \tau_0$, the mean visibility $\langle V^2 \rangle^{1/2}$ is reduced

to $\simeq 0.46$. High precision visibility measurements are usually made in the regime $d \ll r_0$ and $\tau \ll \tau_0$, for which an approximate expression for the mean visibility is (cf 167) $V \simeq \exp[-1.03(d/r_0)^{5/3}]\exp[-0.5(\tau/\tau_0)^{5/3}]$. Note that low visibility bias and high fringe-tracking sensitivity are not incompatible. Large apertures and long coherent integration times can be used for the wideband fringe-tracking channel, where visibility biases are unimportant, while stopped-down pupils and shorter coherent integration times can be used for the passive amplitude channels.

If the visibility biases were fixed, calibration would be straightforward. However, the atmospheric visibility biases fluctuate due to finite averaging over the random process, as well as the time-variability of the turbulence, zenith-angle effects, etc. In addition, there are other nonstationary visibility biases including guiding errors, delay-line jitter, detector dark count, and polarization mismatches, in addition to static biases due to fixed wavefront aberrations. However, with careful calibration, high precision measurements are possible. The approach taken with the Mark III includes rapid star switching and frequent observation of small-diameter calibration stars. With sufficient reference-star observations, one can also fit a calibration constant which is a function of time, zenith angle, or other parameter. It should be noted that given the relatively bright limiting magnitude of a ground-based interferometer, the choice of the calibration stars, as well as the estimation of their a priori diameters, is an important part of the observing plan (109).

Table 1 shows the most recent diameter results from the Mark III (109). The data were carefully calibrated as discussed above. These results used mostly the variable baseline with baseline lengths up to 31.5 m. The diameters, for 12 stars larger than 4.12 mas (limb darkened), have typical formal errors of 1%.

Many observations, such as measurements of the pulsations of cepheids, require diameter measurements with accuracy better than 1%. As described above, visibility errors are dominated by phase errors in the interfering wavefronts. Recent experiments show promise for the use of single-mode fibers after the beam combination optics as spatial filters for those wavefront aberrations (140).

BINARY STARS The observation of binary stars with long-baseline interferometry is particularly interesting (98). With the high angular resolution available, many spectroscopic binaries can now be resolved. Interferometry can independently determine all seven geometric orbital elements of a binary system. Interferometry can also provide accurate magnitude differences between the components as well as their angular diameters. In conjunction with spectroscopic and photometric measure-

Table 1 Recent stellar diameter results with the Mark III [from (109)]

Name	θ_{UD} (mas) 800 nm		θ_{UD} (mas) 450 nm		θ_{LD} (mas)
δ And	3.927	±0.038	3.638	±0.040	4.12
α Cas	5.297	±0.053	4.918	±0.051	5.64
β And	12.783	±0.128	11.535	±0.159	13.81
γ^1 And	7.328	±0.073	6.572	±0.097	7.84
α Ari	6.412	±0.064	5.855	±0.068	6.85
α Cet	12.254	±0.158	11.325	±0.285	13.23
α Tau	19.689	±0.196	18.467	±0.540	21.21
α Ori	49.401	±0.237			
α CMi	5.261	±0.053	5.139	±0.051	5.51
β Gem	7.545	±0.075	7.129	±0.071	8.04
ϵ Cyg	4.340	±0.037			4.62
β Peg	16.618	±0.059	15.996	±0.200	17.98

ments, the fundamental physical parameters of the system, including masses, luminosities, colors, and distance, can be determined. In addition, for binaries for which the components can be resolved, their linear radii and effective temperatures can be determined.

The visibility relationship for binary stars is given by (117):

$$V^2 = \frac{1}{(1+R)^2}[(\Gamma_1)^2+(\gamma R\Gamma_2)^2+2\gamma R\Gamma_1\Gamma_2\cos(k\bar{\mathbf{B}}_p\cdot\bar{\mathbf{d}})], \quad 4.$$

where $\bar{\mathbf{d}}$ is the angular separation vector between the two components, $\bar{\mathbf{B}}_p$ is the projected baseline vector, R is the intensity ratio between the components, Γ_i is the intrinsic visibility of each component as given by the Airy function (Equation 3), and k is wavenumber. The factor $\gamma(k\bar{\mathbf{B}}_p\cdot\bar{\mathbf{d}}, R)$ represents the residual coherence loss caused by the finite width of the bandpass; as the binary star can extend over many interferometer resolution elements, narrow spectral channels are required. Equation 4 defines a sinusoidal grating in the u–v plane. As the interferometer baseline sweeps through the u–v plane with Earth rotation, the visibility fluctuates between $(\Gamma_1 \pm R\Gamma_2)/(1+R)$ (for narrow bandpasses), as shown in Figure 4.

Observational procedures, initial data processing, and calibration for

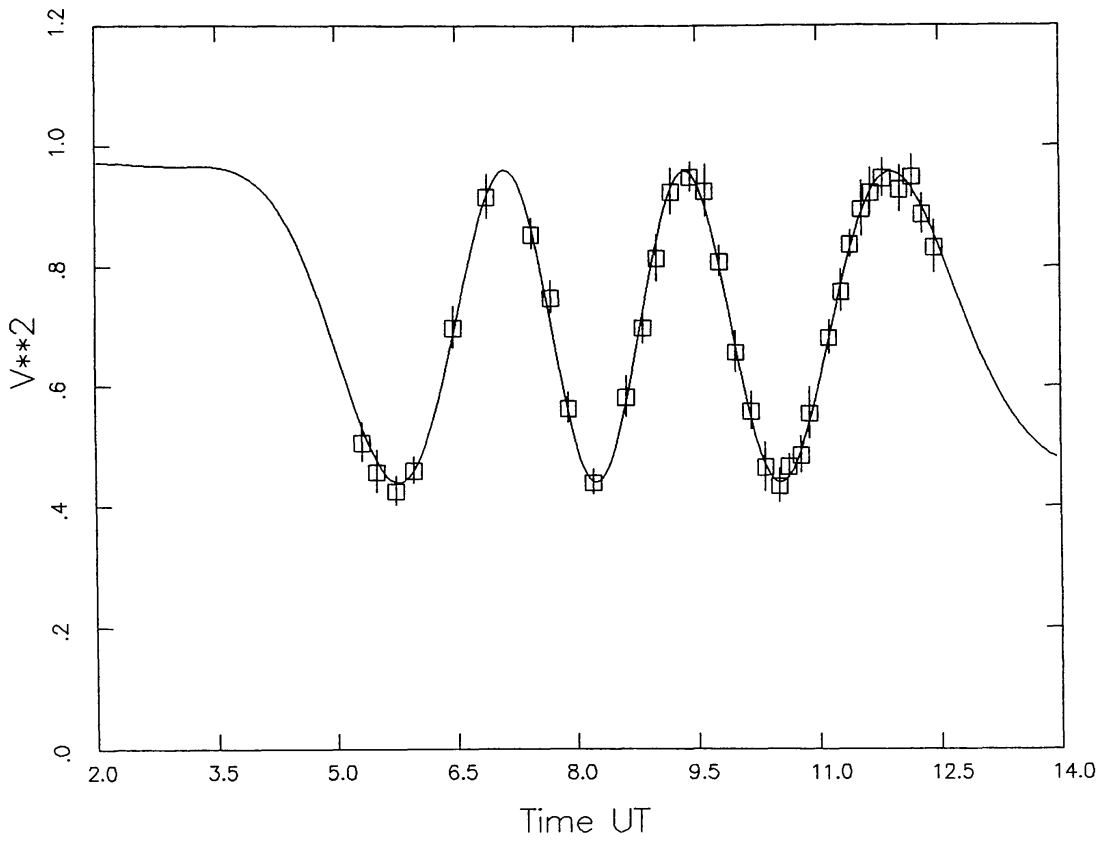

Figure 4 Measured and best-fit squared visibility amplitude vs time at 800 nm for α And observed 31 Aug 89 with the Mark III on a 31.4 m baseline (117). The binary separation for this night is −15.94 mas RA, 5.17 mas dec; the magnitude difference is 1.82 mag.

binary-star observations are similar to those used for the determination of stellar diameters. However, while fast star switching is extremely useful for diameter measurements, it is essential for the observation of binary stars, as the visibility changes rapidly with time on the longest baselines. From the calibrated visibilities for each night, the angular separation vector $\bar{\mathbf{d}}$ and the intensity ratio R are determined from a nonlinear least-squares fit to the data in each of the various spectral channels. From measurements at different times during the period of the binary, the orbital parameters are determined using least squares methods.

Figure 5 shows the orbit of the spectroscopic binary β Arietis as determined with the Mark III interferometer (116, 118). Despite the lack of the object phase, the individual data points are quite accurate: ~0.2 mas in RA and dec. As β Ari is a double-lined binary, the physical parameters of the system, including the masses, are also determined. Presently more than 20 spectroscopic binaries have been resolved with the Mark III, with semi-

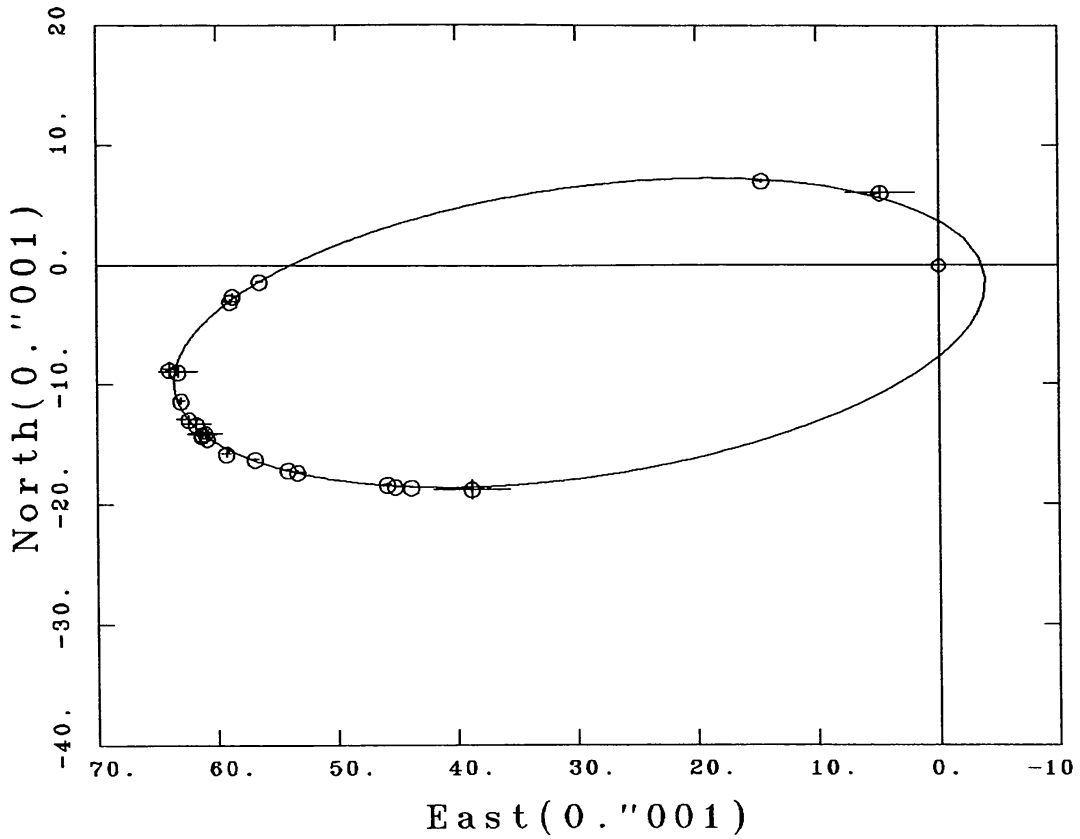

Figure 5 Apparent Orbit of β Ari determined with the Mark III (118). Combined with spectroscopic data, masses $M_1 = 2.34 \pm 0.10$ and $M_2 = 1.34 \pm 0.07$ $M_\odot$, and parallax $\pi = 0.053'' \pm 0.002$, are determined.

major axes larger than 6 mas, and magnitude differences less than 4 mag. Included among these binaries is θ^2 Tau, the brightest binary in the Hyades cluster, for which a preliminary (direct) distance of 43.7 ± 2 pc has been determined (148). Binary star observations should prove to be a fruitful area for future interferometric observations.

While these results, using phaseless reconstructions from two-element interferometers, perhaps pale in comparison with the images routinely produced by radio interferometry, optical interferometry today is still in its infancy when compared with radio interferometry. However, the next generation interferometers will attempt to advance the state of the art in optical interferometric imaging by employing techniques from radio interferometry.

2.4 *Advanced Techniques*

ACTIVE AND PASSIVE INTERFEROMETRY Interferometer operation can be divided into active and passive (absolute) modes (134, 135, 150) depending

on the signal-to-noise ratio (SNR) per coherence volume. The coherence volume is defined as $d^2\tau$, where d is the subaperture diameter, $d < r_0$, and τ is the coherent integration time, $\tau < \tau_0$. The SNR for measurement of visibility or phase with an interferometer is given by (167)

$$\mathrm{SNR}_{V,\phi} = \sqrt{\frac{nV^2}{1+1/(nV^2)}}, \qquad 5.$$

in the photon-noise-limited regime (visible wavelengths), or by

$$\mathrm{SNR}_{V,\phi} = \sqrt{\frac{n^2V^2/b}{1+1/(n^2V^2/b)}}, \qquad 6.$$

in the background-limited regime (infrared wavelengths). In these expressions, n is source photons per coherence volume (one aperture) per spectral channel, b is background photons per coherence volume, and V is fringe visibility (amplitude). Thus active mode is characterized by an SNR $\gg 1$—the photon-rich regime—for which SNR is proportional to $\sqrt{nV}$ at visible wavelengths and to nV in the infrared. Passive mode is characterized by an SNR $\ll 1$—the photon-starved regime.

In active mode, sufficient SNR is acquired per coherence volume to measure the fringe phase in a wideband channel. This information can be used to co-phase the interferometer, by, for example, tracking the white-light fringe, so that pathlength errors (or pathlength uncertainties) are <1 rad rms. Thus, for measurements in other spectral channels, the effect is that $\tau_0 \to \infty$, so that long coherent integration times can be synthesized. Thus even narrow spectral channels can work in the photon-rich regime. Two-color processing on the Mark III uses this coherent technique to synthesize 50–100 ms coherent integration times for the narrowband astrometric channels (148); planned spectral-line observations will also use this technique (110). Co-phasing can also be exploited in an incoherent manner by allowing the use of much wider spectral channels for precise amplitude measurements than would be possible in passive mode; for example, the narrowband channels on the Mark III for imaging in the continuum typically use a spectral resolution $R = 20$–40.

In passive, or absolute, mode, the SNR per coherence volume is too small to measure the fringe phase, either due to a low photon flux n, or to a low fringe visibility V because the source is resolved. As the atmospheric phase fluctuations are not tracked out, coherence for visibility measurements can only be maintained by using narrow bandpasses. The width of

the bandpass required to maintain coherence is set by the amplitude of the atmospheric phase fluctuations, and depends on the baseline length B. The amplitude of these fluctuations is given by (52)

$$\sigma_\phi = \sqrt{6.88}\left(\frac{B}{r_0}\right)^{5/6} \text{ rads rms.} \qquad 7.$$

These fluctuations can be quite large: ~ 70 μm rms for a 100 m interferometer and 1″ seeing. The spectral resolution required to maintain coherence is $R \sim \sigma_\phi$, or ~ 1000 for this example. At this resolution, $\langle V^2 \rangle$ is reduced to ~ 0.9 by the atmospheric fluctuations.

In general, passive operation of an interferometer is far less desirable than active operation. Dividing the n photons per coherence volume among R spectral channels, and then incoherently combining the spectral channels leads to passive-mode SNRs of $nV^2/R^{1/2}$ at visible wavelengths, and $n^2V^2/bR^{3/2}$ in the infrared. Thus, SNR drops rather precipitously for faint objects, or extended objects with low visibility. To increase the SNR, one can average over many coherence times. One can also average over many coherence areas, by using larger apertures, and processing each d-sized patch of the larger aperture independently (either in the pupil or image planes). Thus, if t is the total integration time, and D is the large aperture diameter, then the passive mode SNR is increased by $M^{1/2} = (D/d)(t/\tau)^{1/2}$, where M is the number of frames.

In addition to visibility, other quantities can be averaged in passive mode. For example, the mean group delay of the fringe envelope can be measured (150). In this case, the fringe pattern is dispersed across a photon-counting camera, and the autocorrelation of the fringe pattern, or equivalently its power spectrum, is accumulated over many frames, similar to speckle interferometry. The peak of the accumulated power spectrum gives the mean group delay of the source for use in astrometry. The SNR for group delay is essentially the same as that for visibility (30). Using 1 m apertures, it is possible to achieve a limiting magnitude sufficient to detect the brightest quasars, in order to provide reference objects that can be tied to radio VLBI.

Finally, closure phase can also be measured in passive mode (150). Closure phase, discussed below, is independent of the atmosphere, and thus can be averaged from frame to frame. More precisely, as the conventional phase estimator is badly biased at low SNR, it is the triple product of the fringe quadratures $\exp(i\phi_{12})\exp(i\phi_{23})\exp(i\phi_{31})$—an unbiased quantity—that is averaged. Assuming, for simplicity, that the fringe visibility on each baseline is identical, then the SNR for closure phase (SNR $\equiv 1/\sigma_\phi$) is given by

$$\mathrm{SNR} = \left[3\left(\frac{2}{nV^2}\right)+6\left(\frac{2}{nV^2}\right)^2+4\left(\frac{2}{nV^2}\right)^3\right]^{-1/2} \quad 8.$$

in the photon-noise-limited regime, and by

$$\mathrm{SNR} = \left[3\left(\frac{2b}{n^2V^2}\right)+6\left(\frac{2b}{n^2V^2}\right)^2+4\left(\frac{2b}{n^2V^2}\right)^3\right]^{-1/2} \quad 9.$$

in the background-limited regime. In both expressions, it is assumed that the photons per aperture are split two ways. In the photon-rich regime, the SNR for closure phase is similar to that of visibility. However in the photon-starved regime, the SNR for closure phase is proportional to $n^{3/2}V^3$ when photon-noise limited, and n^3V^3 when background limited. When photon starved, V^3 is just the product of the visibilities on three baselines. Thus, more so than for visibility, the SNR for closure phase falls precipitously for resolved objects, and imaging strategies need to take this behavior into account.

In all passive-mode observations, the interferometer must set the theoretical delay for the object to a higher precision than the atmospheric phase fluctuations. In practice, this will require real-time baseline calibration through astrometry on bright sources, and then a delay offset to the target. In addition, accurate astrometry on the source to much better than the atmospheric fluctuations, $\sim$20–50 mas, will be required. The fundamental positions of faint astrophysical objects are not generally known to this level of accuracy. Thus for the imaging of very faint objects, either the interferometer must be able to do faint-object, wide-angle astrometry, or else the source position must be measured with a dedicated astrometric interferometer.

ADAPTIVE OPTICS Some of the recent work on proposed interferometer systems has considered the use of adaptive optics to phase the individual interferometer apertures in order to use large telescopes efficiently (8). An adaptive-optics system has two key components (67): a wavefront sensor, which measures the atmospheric phase distortions across an aperture, and a deformable mirror, which uses the processed sensor outputs to correct for the distortions in real time. The required number of sensor channels, as well as the required number of degrees of freedom of the deformable mirror, is $\sim(D/r_0)^2$, while the time scale of the correction is $\sim\tau_0$. To sense the phase distortions, the adaptive-optics system uses a reference object nearby the target object. "Nearby" is quantified as being within the isoplanatic patch (78, 133), whose radius (isoplanatic angle) is that angular separation between objects for which the atmospheric fluctuations are correlated to $\sim$1 rad rms. The isoplanatic angle, which is a function of

the seeing and its height distribution, is $\sim 2''$ at visible wavelengths. Like r_0 and τ_0, the isoplanatic angle increases with wavelength as $\lambda^{6/5}$. The end result of the application of adaptive optics is that an entire aperture $D \gg r_0$ can be used coherently, with a limiting magnitude for active operation increased by $(D/r_0)^2$.

The key problem with adaptive optics is the availability of reference stars. The limiting magnitude of an adaptive-optics system is similar to that of an active-mode interferometer: An SNR $\gg 1$ is required per coherence volume. For visible observations and visible sensing, the limiting magnitude for an adaptive-optics system is the same as that of a visible-wavelength active interferometer, ~ 10 mag; the chance of finding a ~ 10 mag object within a $2''$ isoplanatic angle around the target is very small.[2] In addition, the technical challenges are also severe. To correct large telescopes in the visible requires many sensor and actuator channels, and bandwidths of order 100 Hz.

The situation changes dramatically at longer wavelengths, with their larger isoplanatic angles and coherence volumes. Since atmospheric phase effects are mostly achromatic, the sensing wavelength can be chosen independently of the target wavelength. Thus, if the sensing is at visible wavelengths, and the observations are in the infrared, then the wavefront sensor can use much fainter stars. For example, for a target wavelength of 3.4 μm, the coherence volume $r_0^2\tau_0$, $\propto \lambda^{18/5}$, is increased over that at visible wavelengths by a factor of 700, so that a ~ 17 mag reference star can be employed. This star can now be located within the isoplanatic patch at 3.4 μm, $\sim 18''$, providing a factor of 80 larger search space than at visible wavelengths. Thus, using natural sources, adaptive optics can be employed over most of the sky at infrared wavelengths (9). The technical challenges are also less severe at the longer wavelengths. Phasing a 10 m telescope at 3.4 μm requires ~ 130 degrees of freedom in sensing and actuation for $1''$ seeing; less at a good site. On the other hand, the number of degrees of freedom also represents the sensitivity gain obtainable with adaptive optics.

A special case of adaptive optics is tilt correction. While $(D/r_0)^2$ is the proper expression for degrees of freedom when $D \gg r_0$, a different result applies at the other extreme. In particular, for $D < 3.4r_0$, tip-tilt correction yields a diffraction-limited system ($\langle V^2 \rangle \sim e^{-1}$) (53), and for longer wavelengths may be all of the adaptive optics required.

[2] Note that for the case of imaging a large, extended object, good closure phase SNRs may require a fairly large integrated flux, and thus the object itself, unresolved by the subapertures, can serve as the reference, providing a significant sensitivity gain (D. Mozurkewich, personal communication).

While adaptive optics has been studied by the defense community for many years, recent experiments within the astronomical community (129, 137), as well as some defense policy shifts, promise to bring the cost of these systems within the range of astronomers.

To extend the gains of adaptive optics to shorter wavelengths requires a means to increase the availability of reference sources. Synthetic beacons, or laser-guide stars, provide an artificial reference source near the target using compact laser scattering from the clear atmosphere at an altitude of several kilometers (Rayleigh beacon), or from the mesospheric sodium layer at 92 km (sodium beacon). While recently proposed within the open literature (51), and with some preliminary experimental results (55, 171), recently declassified work has revealed that the defense community has been working in this area for some time, with some impressive results on small telescopes (54, 123). Currently, several groups are studying the application of this technology to astronomical observations.

While adaptive optics addresses the problem of increasing the coherence area, the sensitivity of an interferometer is also limited by the coherence time τ_0. In principle, a natural reference star within the isoplanatic patch can also be used to co-phase the interferometer. Because of the need to fringe track, the source must be detected within the coherence volume of the sensing wavelength, and thus this technique is limited to longer wavelengths. However partial co-phasing, using a source outside of the isoplanatic patch, can allow passive operation with much larger spectral channels than would otherwise be possible (7).

INTERFEROMETRIC IMAGING As discussed earlier, atmospheric phase effects are very large at optical wavelengths. Thus, the measured fringe phase with a two-element interferometer, while important for co-phasing and astrometry, is not useful for imaging. Consequently, amplitude-only imaging has been employed with the present generation of two-element interferometers, as discussed previously. True nonparametric imaging requires the use of the object phase, or a closely related quantity. That related quantity is the closure phase (119), which is the sum of phases around a closed loop of three telescopes. With closure phase, the atmospheric errors—"telescope-dependent errors"—will cancel, while the object phases, which are baseline dependent, will add. Closure phase, long used in radio astronomy to yield high dynamic range images, was proposed for use at optical wavelengths by Rogstad (136). Presently, the astronomical application of closure phase at optical wavelengths has only been demonstrated using a masked pupil on a large telescope (66); the closely related (131) technique of triple correlation (180) employed in speckle interferometry has also been used to reconstruct images using the object

phase on a large telescope. The application of closure phase among independent apertures at optical wavelengths is one of the goals of the next generation of ground-based instruments.

The measurement of closure phase requires simultaneous combination of three or more apertures. The next generation of interferometers designed for imaging will employ multiple telescopes or siderostats with multiway beam combiners to simultaneously measure the fringe parameters on three or more baselines. With more than two apertures, the number of options available in beam combination and signal processing are greatly increased. However, there are probably two major approaches to multiple-aperture optical imaging: pairwise (Michelson) or Fizeau combination.

Pairwise (Michelson) combination This approach is most similar to that used in radio interferometry. In its simplest implementation, with an n-element system, the light from each aperture is split $n-1$ ways, and fringes on all $n(n-1)/2$ available baselines are measured simultaneously. Unfortunately, as discussed above, signal splitting at optical wavelengths is costly. For this hypothetical n-element system, the active-mode limiting magnitude for each baseline pair is reduced by $n-1$ over that of a simple two-element interferometer. Furthermore, the active-mode SNR is proportional to the intrinsic object visibility, $\sim 1/\sqrt{p}$ at visible wavelengths, where p is the number of resolved points in the object. Thus, on those baselines where the object is resolved, the active-mode limiting magnitude is still further reduced. While passive mode operation is always possible, it is clear that with its strong dependence on n and V, prohibitively long integration times may be required.

Because of the behavior discussed above, some operational scenarios that seem contrary to radio interferometry experience have been developed. In the radio, typically a mostly nonredundant array geometry is used in order to get as many different u–v plane points as possible, and all possible baseline pairs are interfered simultaneously (170). In one scenario for optical imaging, rather than interfering all baselines simultaneously, the array is divided into several subarrays, each with at least three telescopes, in order to minimize signal splitting so that the individual baselines work in the photon-rich regime. Another scenario uses highly-redundant arrays (132). The idea is to have longer baselines spanned by a number of shorter ones, and to use pairwise observations on the shorter baselines where the object is less resolved to "bootstrap" the way to co-phasing of the longer baselines. Once the interferometer is co-phased, long coherence times can be synthesized for the baselines with low SNRs. Because of error propagation, while the longer baselines may not be completely co-phased, they will only be partially incoherent. Thus, passive

mode operation, but with relatively large spectral channels, can also be used to average amplitudes and closure phases.

In a pairwise optical interferometer, the instantaneous field of view is set by the spectrometer resolution, which must be greater than the number of resolved points across the object. (Again, as mentioned above, a white-light channel is still used for co-phasing, while the spectrometer is used for the science measurements.) Beam combination in a pairwise interferometer can be accomplished in either the pupil plane by using beamsplitters, or in the image plane with a combining telescope. In the latter case, the interferometer beams are arranged in a nonredundant configuration at the telescope entrance pupil (3); the nonredundant spacing results in a unique spatial frequency for each fringe pattern in the image plane, so that the fringes from different baseline pairs can be separated using Fourier analysis. An alternative pupil-plane technique is the use of fiber-optic beam combiners using optical couplers to divide the light from each aperture among baselines (139). In this case, dispersion due to fiber-length mismatches must be carefully controlled in order to allow wideband operation. All of these approaches are compatible with spectrometers to set the field of view. As an alternative to dispersive spectrometers, Mariotti & Ridgway (96) have proposed the use of double Fourier interferometry, where the spectral information is extracted from FTS spectroscopy on the combined beams.

Fizeau combination Fizeau combination is equivalent to imaging with a sparse-aperture telescope. Essentially, the various interferometer subapertures are reimaged at the pupil of a combining telescope in exactly the same orientation, and with a consistent scale, as they are seen by the incident wavefront. While this task is nontrivial, even when the subapertures are mounted on a single pointing structure (179), it becomes quite complicated when the subapertures are fixed and delay lines are used to "point" the interferometer. In both cases, the tolerances involved are those of constructing a diffraction-limited telescope from individual segments: The tolerances are not only in piston, but also in scale and the x, y positions of the reimaged apertures. When the subapertures are fixed, the reimaging must be dynamic as the projected array geometry varies with the source elevation (103). However, if done correctly, the field of view of the resulting system is set by the aberrations in the equivalent optical system, rather than by the spectrometer resolution. As the interferometer now looks like a telescope, such techniques as triple correlation can be applied to retrieve information from the combined image (128). These techniques are applicable even if the apertures are not phased, or the interferometer is not co-phased, although there is the corresponding pas-

sive-mode SNR penalty. As the aperture is now sparse, there is incomplete u–v coverage, and hence large sidelobes, which must be accounted for in the signal processing. Because of the difficulties associated with Fizeau combination, initial operation of the next generation imaging interferometers will likely use pairwise combination, in either the pupil or image planes.

INTERFEROMETRIC ASTROMETRY

Wide-angle astrometry Wide-angle astrometry has traditionally been accomplished with transit instruments and astrographs (79). A significant advantage of optical interferometers over these instruments is the longer baselines available, and the correspondingly longer lever arms over which linear errors make their effects known. This is similar to the advantage held in radio astrometry and geodesy by VLBI techniques. In addition, interferometers have a simple geometry which can be monitored. However the atmosphere establishes the fundamental limit to accuracy on the ground.

The rms error σ_α in an absolute measurement is a function of the integrated turbulence strength. Assuming an infinite outer scale Kolmogorov atmospheric model, valid for moderate baselines, the atmospheric error for moderate integration times t is given by (cf 91)

$$\sigma_\alpha \simeq 0.25 t^{-1/6} \text{ arc sec}, \quad t \gg B/V, \tag{10.}$$

for average (1″) seeing. This result is independent of baseline, at least until the outer scale of turbulence is reached, and clearly depends only weakly on integration time. It is also equally applicable to telescopes and interferometers. For 90-sec integrations, this result yields ~ 120 mas per point. Observations with the Mark III, after constant-term calibration, but before two-color correction, yield approximately 50 mas per 90-sec point, consistent with the excellent seeing ($<0.5''$) for those observations (147). For star-switched measurements, these points decorrelate between switching cycles, for a nightly error reduced by the square root of the number of cycles. Two-color techniques, applicable at visible wavelengths, can provide a further improvement in performance, as discussed above.

Narrow-angle astrometry The nature of the atmospheric angle-of-arrival fluctuations greatly favors narrow-angle astrometry. Over narrow angles, the atmospheric fluctuations remain correlated, resulting in smaller errors for differential than for absolute measurements. In addition, the "whitening" effect of differential measurement yields an astrometric error which decreases as white noise, i.e. as $\sqrt{t}$, rather than as $t^{1/6}$ for an absolute measurement. The atmospheric error σ_δ for a simultaneous differential measurement between stars separated by angle θ is given by (cf 91)

$$\sigma_\delta = 1.86\theta^{1/3}t^{-1/2}\,\text{arc sec}, \quad \theta h^* \gg B, \quad t \gg \theta h^*/V^*, \tag{11.}$$

$$\sigma_\delta = 823B^{-2/3}\theta t^{-1/2}\,\text{arc sec}, \quad \theta h^* \ll B, \quad t \gg B/V^*, \tag{12.}$$

where B is baseline, V^* is a mean wind speed, and $h^* \sim 6$ km is a mean atmospheric height. This expression assumes a standard 1″ Kolmogorov turbulence model and a constant 10 m/s transverse wind; lower errors should be possible at a good site. As seen from Equations 11–12, there are two regimes, depending on the linear separation θh^* between the beams from one interferometer aperture at atmospheric height h^*. When this separation is larger than the baseline length, the rms differential error is independent of baseline length, and depends on star separation to the 1/3 power. When this separation is smaller than the baseline length, the rms error is inversely dependent on baseline length to the 2/3 power, and linearly dependent on the star separation. From this expression, it is clear that there is a significant advantage to long baselines (or telescope diameters). In particular, with long baselines, the error performance in the very narrow angle regime improves with baseline as $B^{2/3}$; in addition, the breakpoint between the narrow and very narrow angle regimes moves to larger separations.

The results above assume simultaneous measurements of the two stars. Ordinarily, the field of view of a Michelson interferometer is limited to the diffraction limit of the subapertures. One way to implement a differential measurement is with a pair of parallel interferometer baselines, separated by distance b, each looking at one of the target stars. In this case, the rms error will decrease with decreasing star separation until $\theta h^* = b$. A second implementation is to use a single interferometer with two delay lines, and a dual-star feed for each aperture which feeds two stellar beams along nearly parallel optical paths.

Over narrow angles, the availability of reference stars becomes problematic. However, in some sense this problem is the reverse of the adaptive-optics problem: One must typically find (faint) reference stars near a bright target, rather than a bright reference near a faint target. Thus the bright target can be used to co-phase the interferometer over the isoplanatic patch. When co-phased, the coherent integration time for stars within the patch is increased, in theory to arbitrary values, greatly increasing the limiting magnitude of acceptable reference stars, especially for observations in the near-infrared. For narrow-angle astrometry, interferometry has to compete with filled-aperture astrometry on the next generation of large telescopes. While telescopes allow for simultaneous observations of multiple reference stars, an interferometer, although limited to pairwise observation, has a reduced atmospheric error by virtue of its longer possible baseline, with ultimate limits in the 10's of microarcseconds.

2.5 *Future Instruments*

There are a number of interferometer projects in the planning or development stage. SUSI (Sydney Univ. Spatial Interferometer) (39, 40), under development in NSW, Australia, is a two-element interferometer with extremely long baselines—to 640 m. Science goals for this instrument include the determination of the stellar diameters of main-sequence stars.[3] The SUSI prototype was discussed earlier. IOTA (Infrared/Optical Telescope Array) (28, 125), under development at Mt. Hopkins, is a three-element (initially two) interferometer for visible/infrared observations. Initial baselines will be up to 45 m. A multiple telescope optical interferometer array has also been proposed at Georgia State University (97, 99). This instrument would use seven, 1 m telescopes in a 200 m Y-shaped array.

There are presently two interferometers under development by the U.S. Naval Research Lab and the U.S. Naval Observatory. As currently planned, the Big Optical Array (108) will operate at visible/near-infrared wavelengths using six siderostats, relocatable at fixed stations in a Y-shaped array with a radius of 250 m. The instrument will initially use two, 3-way beam combiners to measure closure phase for imaging. The Naval Observatory Astrometric Interferometer (68, 69) will be a four-element interferometer designed primarily for astrometry. With orthogonal baselines of $\sim$25 m, the key feature of this instrument will be the extensive use of laser metrology to continuously monitor the delay constant, as well as the three components of the baseline vector, using deeply buried optical anchors.

One of the most ambitious of the interferometer projects under development is the Very Large Telescope (VLT) Interferometer (4–8, 103). This is one of the operating modes of the VLT array, under development by ESO, on Cerro Paranal, Chile. Besides operation as a set of four independent 8 m telescopes, and as an incoherent array of four telescopes to increase light-gathering capability, operation of the VLT as an interferometer is planned. Initial operation will probably use pairwise, image-plane combination, while a Fizeau combiner is planned for future wide-field operation. In addition to the 8 m telescopes, 2–4 movable $\sim$1.8 m auxiliary telescopes will also be added to improve u–v coverage for imaging. The 8 m telescopes will employ adaptive optics in their coude trains for pupil phasing at $\lambda > 2.2$ μm.

In the U.S., with the recently funded Keck II telescope, interferometric combination between the two Kecks and a number of outrigger telescopes

[3] Note added in proof: Initial operation of SUSI has begun; see 9a.

is also being planned (100). The baseline concept is similar to that of the VLT interferometric mode, including coherent combination of the two Kecks as a two-element interferometer using adaptive optics at infrared wavelengths. The addition of 3–4 movable outrigger telescopes, which can function as a stand-alone array, will allow for high-resolution synthesis imaging of such objects as protoplanetary disks. Long-baseline narrow-angle astrometry for indirect planet detection using the outriggers is also being considered.

3. INTERFEROMETRY IN SPACE

In the previous section, the problems and potential solutions for ground-based interferometers were discussed in some detail. On the ground, optics technology has progressed to the point where the major technical challenges concern the atmosphere. However, despite the numerous advanced techniques that can be applied to overcome the effects of atmospheric turbulence, some fundamental limitations remain.

3.1 *Fundamental Advantages of Space*

Space has advantages for astronomy that are well known. The lack of an atmosphere means that observations can be made over the whole optical-infrared spectrum from the far UV (110 nm) to the far infrared (300 μm). However, besides opening up the electromagnetic spectrum, space provides several unique advantages for long-baseline interferometry.

For astrometry with a ground-based interferometer, it was shown earlier that the atmosphere is the fundamental limitation to accuracy. In space, the elimination of the atmosphere means that astrometry over wide angles is possible with extreme precision.

For the case of imaging with a ground-based interferometer, the use of adaptive optics, laser guide stars, and other advanced techniques can at most poke a small hole in the atmosphere. High resolution visible-wavelength images are limited to a field of view of a few arcsec—the size of the isoplanatic patch. The elimination of the atmosphere for a space interferometer means that imaging over wide fields at high angular resolution is possible. In addition, it is also unknown at present how well the laser guide star technique will work in normal ground-based observations, and for what wavelengths. The ultimate wavelength limit for adaptive optics with laser guide stars is set by the wavelength at which the diffraction from an r_0-sized aperture equals the isoplanatic patch size. Although this is in the UV at a good site, some estimates have suggested that the laser guide star technique will only be usable at wavelengths longer than ~ 0.8 μm due to difficulties with sodium-layer saturation and other problems.

An interferometer in space suffers from no such difficulties, and diffraction-limited images in the blue and UV are possible.

Compared with ground-based telescopes and interferometers, there are also significant advantages to space for imaging in the thermal infrared (1, 2, 11, 21, 23). By cooling the optics, the thermal background of a space instrument can be reduced to the level of Zodiacal light. The reduction in background between a 0.1 emissivity, 275 K, ground-based instrument, and one limited by the 2×10^{-7} emissivity of the Zodiacal light, leads to a 3 order-of-magnitude improvement in sensitivity. In the far future, large-aperture, low-temperature interferometers in space (and only in space) will be able to detect the thermal radiation of Earth-like planets around nearby stars (1, 141, 143).

In addition to wide-angle astrometry, and high sensitivity wide-field imaging, there is one more fundamental advantage of space. In space the incident wavefront is essentially perfect, many orders of magnitude better than $\lambda/20$. The perfection and stability of this wavefront makes possible hyper-contrast imaging (141, 144, 169). In a later section we describe a concept for a starlight cancellation interferometer that takes advantage of the wavefront quality in space for imaging faint objects next to bright ones.

3.2 *Technical Challenges for Space Interferometry*

While space interferometry has great potential, there are significant technical problems in operating a long-baseline interferometer in space. The first is size. While it is possible to build an interferometer with a baseline of 1–3 m, its photon-noise-limited performance would not match that of the Hubble space telescope. The fundamental reason for building interferometers in the optical region is economic, the same reason for building interferometers in the radio. To first order, interferometers make sense when building a telescope of the equivalent resolution would be too expensive.

Long baselines require that the interferometer structure be deployed in space after launch. While an interferometer on the ground is attached to the Earth, a solid body that is stable mechanically, a space structure must be necessarily floppy in order to minimize the weight of the structure. However, space itself is a seismically and acoustically quiet environment; the sources of vibration that would cause fringes to be blurred are all on the spacecraft itself. It is possible to operate a floppy space interferometer as one would a ground-based interferometer, with phase uncertainties calibrated by closure-phase measurements. However, as discussed earlier, this entails a significant sensitivity penalty for resolved objects. To justify space-based operation the optics must be phase stable. NASA-funded

technology programs to build and control large space structures at the tens of nanometer level are underway (90).

As long-baseline interferometers will have very high angular resolution, they will also have pointing requirements to match. In space, accurate pointing also requires accurate knowledge of the spacecraft velocity. Often, precise pointing of space instruments is done by looking at nearby guide stars; in this case, the effect of stellar aberration must be accounted for. For Earth-based interferometers, knowledge of the orbital motion of the Earth is required; this is known with extreme accuracy. In space, the orbital motion of the spacecraft around the Earth must also be known with an accuracy of 1 mm/s to 4 m/s depending on the angle between the guide star and the target star, and the degree of pointing accuracy needed. In general, the spacecraft will need an on-board GPS receiver or else be tracked continuously by a ground station.

3.3 *Early Studies of Space Interferometers*

The tremendous potential of space interferometry has been known for a long time and numerous groups have studied a number of possible interferometer configurations since the early 1980s. The architectures of these interferometers can be separated roughly into two broad categories: Michelson and Fizeau. As discussed above, a Michelson interferometer combines light at a beamsplitter, while a Fizeau interferometer is really a dilute-aperture telescope—a telescope where most of the glass of the primary is missing (47). In this case, the optical system forms an image, although one with large sidelobes because of the poor u–v coverage.

The number of interferometer projects studied is quite large, and a partial list is given in Table 2. These projects range from single-spacecraft interferometers with multiple collecting apertures from 25 cm to 2.5 m in diameter, to multiple spacecraft interferometers with baselines to multi-km, to lunar interferometers. A number of workshops (19, 57, 92, 93, 152) and reviews (48) provide a summary of activity in the field. Two concepts which have been studied in some depth, POINTS (Precision Optical Interferometer in Space) (127) and OSI (Orbiting Stellar Interferometer) (145) are discussed below.

3.4 *Astrometry with Space Interferometers*

In 1990, the Astronomy and Astrophysics Survey (Bahcall) Committee (112) formed a panel to look into the scientific potential of interferometers. That panel recommended the construction of ground-based interferometers as well as space-based interferometers. The space-based mission called *AIM*, the *Astrometric Interferometer Mission*, was adopted by the Survey Committee in its recommended mission list.

Table 2 Partial list of space interferometer concepts and approximate parameters

Name	Type	Baseline (m)	Total collecting area (m^2)	Institution
BSE	Michelson	5	0.4	SAO [174, 178, 176]
COSMIC	Fizeau	36	20–50	MSFC, SAO [173, 87, 175, 177]
FFT	Fizeau	25	50	JPL [164, 165]
HARDI	Fizeau	6	1–2	STScil [12, 11, 13]
LASII	Michelson	25	6	Univ. of Colorado [157, 14]
OASIS	Michelson	100	2–3	ESA [113, 115]
OSI	Michelson	20	1.2	JPL [145, 88]
POINTS	Michelson	2	0.2	SAO [124, 127, 126]
SAMSI/VISTA	Michelson	0.1–100 km	2	JPL [156, 155, 74]
TRIO	Michelson	1–20 km	3	CERGA [83, 84, 34]
Michelson	Michelson	50–100	2	ESA [49, 47, 114]
Lunar Int.	Michelson	2 km	15-30	JPL [29, 31, 58, 142]
Lunar Int.	Michelson	>100	>10	ESA [94]

AIM was to be capable of wide-angle astrometry with 3–30 μas accuracy on 20 mag stars. Astrometry was chosen as the first scientific objective of a space interferometer for several reasons. Compared to the current state of the art, wide-angle astrometry promised a two order of magnitude improvement over the *HIPPARCOS* satellite (79), as well as a two order of magnitude improvement over what is ultimately possible from the ground. Astrometry was also chosen because of the large number of areas of astrophysics that would benefit from such a large increase in accuracy.

ADVANTAGES OF INTERFEROMETRY FOR ASTROMETRY The principle advantage of interferometry is its high resolution, which results in the ability to make accurate measurements of faint objects in a short integration time. To first order, the photon-noise-limited accuracy σ_ε is

$$\sigma_{\varepsilon(\mathrm{int})} = \frac{\lambda}{2\pi\sqrt{ntBD}}, \qquad 13.$$

where B is the baseline length, D is the diameter of the individual apertures, n is the photon flux from the star, and t is integration time. This expression can be compared to the case of a filled-aperture telescope:

$$\sigma_{\varepsilon(\mathrm{tel})} = \frac{3\pi\lambda}{16\sqrt{ntD^2}}, \qquad 14.$$

where D is the telescope diameter. In terms of photon-noise-limited per-

formance, a 20 m baseline interferometer with 50 cm apertures is equivalent to a filled aperture telescope with a 6 m diameter.

TECHNICAL CHALLENGES OF SPACE ASTROMETRY Without the atmosphere, it is possible to make extremely accurate astrometric measurements. However, the technical demands on the instrument are significant. By definition, wide-angle astrometry is the measurement of the angle between stars separated by more than the field of view of a telescope or interferometer. Most proposed concepts for space-based wide-angle astrometry use two or more connected interferometer baselines looking at several stars simultaneously. The key to accurate astrometry is the ability to measure or maintain the angle between the two interferometers to microarcsec accuracy. This is done by building a laser interferometer optical truss to connect the interferometers.

For a given level of angular accuracy, the required accuracy of the metrology is inversely proportional to the length of the baseline. While 1 μas astrometry with a 50 m instrument requires 250 pm (picometer) accuracy, a 5 m instrument has a 25 pm requirement. These levels of accuracy are significantly higher than what is available commercially. In addition there are several different types of length measurements that the metrology systems need to make.

As an illustration of the technical challenges that must be overcome, consider the OSI concept (145) developed at JPL, shown in Figure 6. Astrometry with OSI is described by the astrometric relation in Equation 2. In the OSI concept, corner-cube retroreflectors are placed at the siderostat mirror pivots; the vector between two corner cubes defines the baseline vector $\bar{\mathbf{B}}$. Similarly, the distance between the beamsplitter and the corner cubes through the delay lines is measured to give the delay offset C. The validity of this mathematical model at subnanometer levels is crucial to microarcsec astrometry.

OSI consists of three interferometers with collinear baselines. It uses baseline lengths to 20 m, and 0.5 m apertures. Two of the interferometers lock onto guide stars to provide attitude control information. The third interferometer then switches among a number of stars, measuring the position of the delay line at which fringes are found. For microarcsec astrometry, the major technical issue is the laser optical truss that ties the interferometers together. At the picometer level, a number of potential sources of systematic errors must be eliminated. Among them are phase changes due to polarization effects, and pathlength errors due to imperfect optical surfaces and the thermal stability of the optics.

The problem of imperfect optical surfaces is the most challenging. As the siderostats articulate to view different stars, the angle of incidence of

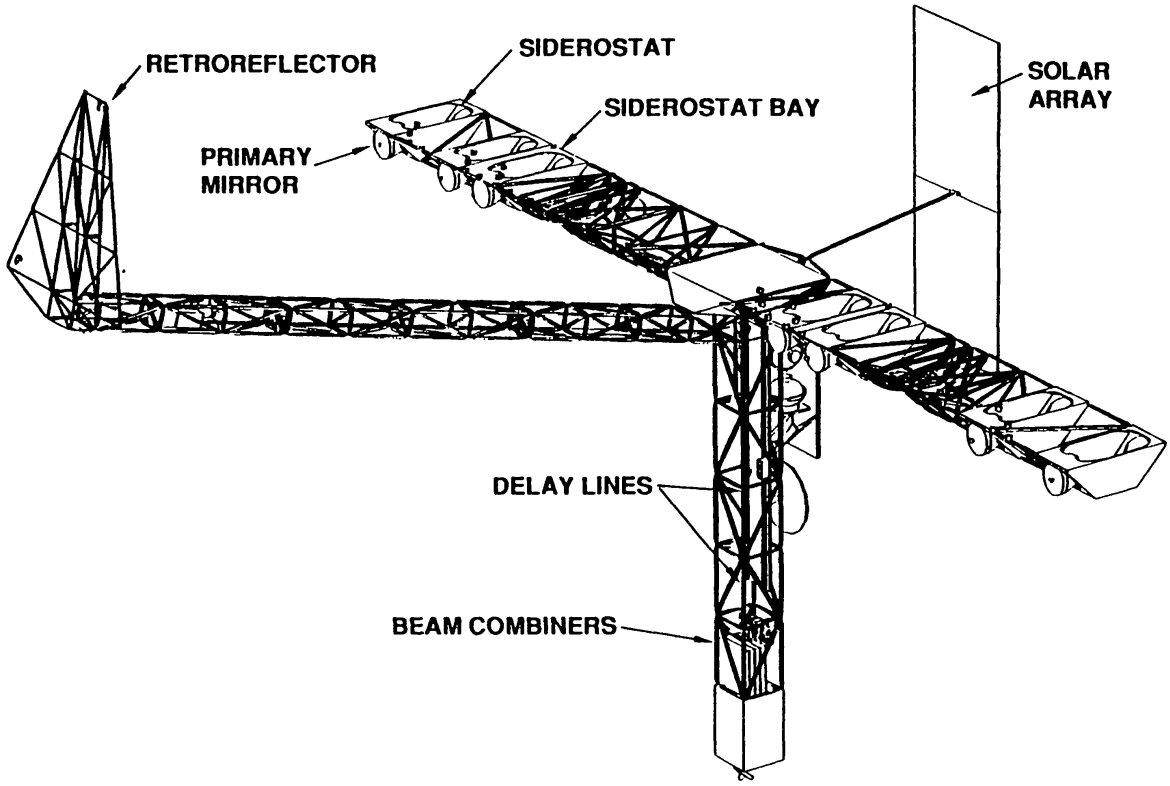

Figure 6 Configuration of the OSI instrument concept.

the laser beams on the optical surfaces will change. However, when laser beams at different angles interrogate a corner cube, they sample different parts of its surface. To the extent that the faces are not perfect at the picometer level, or the faces of the cube are not exactly orthogonal, there will be errors in the laser measurement. Current commercially available state of the art retroreflectors have face alignment accuracies of $\sim 0.5''$ (~ 12 nm wavefront error over a 5 mm laser beam), and surface flatness of $\sim \lambda/100$ (6 nm) rms. Calibration of these error sources at the 0.1% level for 10–100 pm metrology is the major challenge to space interferometry at the 1–10 μas level.

Another concept that has been studied for space astrometry is POINTS (127). POINTS uses two interferometers to look at two stars $\sim 90°$ apart. Instead of using articulating siderostats to point at different stars, POINTS articulates the two interferometers. A laser metrology truss ties the two interferometers together through a set of four fiducial blocks. In order to keep the cost of the instrument low, the nominal design uses a short 2 m baseline with 25 cm apertures. In order to achieve an accuracy of several μas with a much smaller instrument than OSI, the POINTS instrument would limit its targets to stars that are ~ 6.5 mag brighter. Corresponding

to its shorter baseline is a tighter metrology requirement: 1–10 pm vs 10–100 pm accuracy for 1–10 μas astrometry.

3.5 *Imaging with Space Interferometers*

As mentioned above, operation in space has fundamental advantages for interferometric imaging in several areas.

WIDE-FIELD IMAGING Wide-field imaging for a space interferometer can imply fields of view as small as 20″. However, a 20 m baseline interferometer has ~ 5 mas resolution in the visible. So while a ground-based image with a 20″ field has only $\sim 20^2$ pixels, and is not normally considered wide field, for a space interferometer the same image would be $\sim 4000^2$ pixels, placing significant requirements on the camera. Wide-field imaging imposes additional requirements. An interferometer with baseline B samples spatial frequencies at B/λ cycles per radian. The problem is that at different wavelengths, that same physical baseline samples different spatial frequencies, so that the fringes at different wavelengths will be out of phase if the object extends over a finite field of view (FOV). Thus, the spectral range of the detector must be restricted to $\Delta\lambda/\lambda < (\lambda/B)/\text{FOV}$. However, if the individual apertures of the interferometer have diameter D, the field of view can be restricted to λ/D, and the spectral resolution must be limited to $\Delta\lambda/\lambda < D/B$. For very dilute aperture interferometers (large B/D), the spectral restriction can significantly affect the SNR of an image. In that case, an imaging spectrometer must be used to simultaneously record the fringes at many wavelengths simultaneously in order to yield a high SNR.

HIGH DYNAMIC RANGE IMAGING In space, the wavefronts from an astronomical object are very nearly perfect, many orders of magnitude better than the $\sim \lambda/6$ wavefront quality from a properly operating adaptive optics system. On a ground-based adaptive optics system, the image of a star appears as a diffraction-limited peak surrounded by a halo, whose size is equal to the seeing disk; the integrated flux in the halo is typically several times the flux in the diffraction-limited core. In space, instruments like the Hubble telescope, when the problem of spherical aberration is fixed, will have much sharper images. The quality of the images then will be limited by the much smaller irregularities in the wavefront due to errors in the figure of the optics. These figure errors will degrade the wavefront to $\sim \lambda/30$, and although significantly better than a ground-based adaptive optics system, will limit the achievable dynamic range.

The wavefront irregularities produce two kinds of error. First, the image formed by a slightly imperfect optical system will exhibit narrow-angle scattering, which will make it difficult to detect the presence of a dim object near a bright one. To first order, the pattern of scattered light will be

constant and deconvolution techniques can be used to remove most of its effects. The second source of error is fundamental: The scattered light will obey Poisson statistics. These fluctuations place an ultimate limit on the ability of deconvolution techniques to extend the dynamic range of the image.

One scientific reason for high dynamic range imaging is the possible detection of planets around nearby stars. If one were to look at the solar system from a distance of 10 pc, the Sun would be a 5 mag star, and Jupiter and Earth would be 27.5 and 28.5 mag. The key to very high dynamic range imaging is to optically prevent the starlight from being scattered into the position of the planet.

The key element for planet detection is a starlight cancellation scheme to eliminate the star's shot-noise component. The original concept is due to Bracewell (20), although the concept has evolved considerably. However, the basic principle remains to take light from the star at two spatially separated locations and interfere it destructively. The planet light, because it enters the interferometer off-axis, does not suffer destructive interference.

The most obvious scheme for starlight cancellation with an interferometer is to use a scheme like Figure 1, where the paths in the two arms are adjusted to yield a null. However, a conventional interferometer using a single beamsplitter for starlight combination and cancellation has several practical problems. One is that the beamsplitter must have a transmission-to-reflection ratio of exactly 50/50 in order to match intensities before interference. Another is that the pathlengths in the two arms must be different by $\lambda/4$ (because of the beamsplitter phase shift) in order to produce a null; since $\lambda/4$ is a different physical distance for different wavelengths, a deep null is possible only for monochromatic light. Another problem is that imperfect mirror coatings (metal with finite conductivity) will introduce polarization-dependent phase shifts when light is reflected at oblique angles, which will limit the null depth with unpolarized light. However, the most important problem is that wavefront aberrations attributable to imperfect optics will limit the depth of the achievable null.

The nulling concept shown in Figure 7 addresses these problems (141, 143, 144). As shown in the figure, light from two apertures is split at a beamsplitter into two paths, one in plane, one out of plane, reflected from two dihedrals, and then recombined at the beamsplitter. The output of the beamsplitter is fed to single-mode optical fibers. Because the beamsplitter is now used once in transmission and once in reflection in each arm, the beamsplitter no longer needs to be precisely 50/50. In addition, as the null is achieved by a polarization flip rather than by a phase delay, the $\lambda/4$ phase shift is eliminated, and the null is now achromatic. The layout is

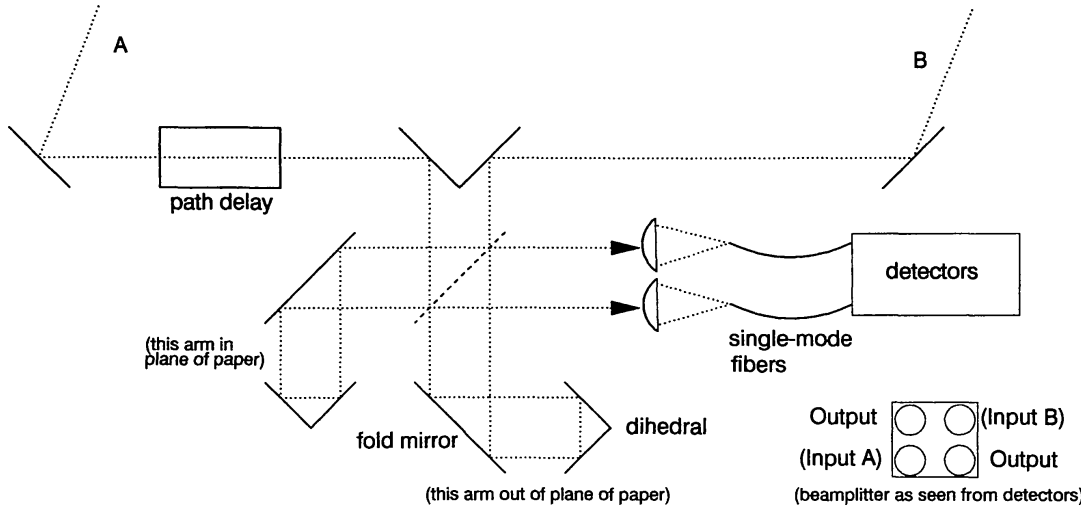

Figure 7 Achromatic nulling interferometer concept.

also symmetric with respect to polarization: Each arm has 2 S-type reflections and 2 P-type reflections. Thus, with identical mirrors in each arm, all polarization effects are eliminated. With slightly mismatched mirrors, the fold angles can be adjusted to tune out the differences. Finally the single-mode fibers serve as spatial filters. As the fibers support only a single spatial mode, scattered light from corrugations in the phase front due to surface imperfections will not propagate, and will escape into the cladding. Thus, if the amplitudes of the propagated fiber modes for the two input apertures are matched, and the pathlengths in the two arms of the nulling interferometer are made equal, complete cancellation should, in theory occur; supersmooth optics with $\lambda/5000$ accuracy are not required.

In the same way that the planet light is not cancelled because it enters the interferometer off-axis, the edges of the star, which are slightly off-axis, will also not be cancelled completely. This limited cancellation for a finite-diameter star is a potential problem because of the deep nulls required for planet detection. For a two-element interferometer, the leakage of the light from a star of diameter θ is given by (1, 144)

$$\text{Leakage} = \frac{1}{8}\left(\frac{\pi\theta B}{\lambda}\right)^2. \qquad 15.$$

The baseline B must be large enough to resolve the planet from the star. For a sun-Jupiter system, the separation of the planet from the star is about 1000 times the radius of the star. With a baseline that overresolves the star-planet system by a factor of 6, the light leakage due to the finite diameter of the star is 7×10^{-5}. To provide a higher degree of cancellation,

Angel (1) proposed the use of a four-element interferometer. Essentially, the light from each of two, two-element interferometers is combined in a third interferometer. In this case, the leakage for a finite-diameter star is greatly reduced, dependent on the fourth power of the star's diameter, and is given by

$$\text{Leakage} = \frac{1}{96}\left(\frac{\pi\theta B}{\lambda}\right)^4. \qquad 16.$$

With the assumptions above, the leakage is now 3×10^{-9}.

While in principle, very deep cancellation of starlight is possible at visible and near-infrared wavelengths, considerable technology development is needed to bring this into practice. However, if a moderate degree of starlight cancellation is achieved, e.g. 10^6, an instrument attached to the Hubble telescope (144) would be able to detect a Jupiter in a sun-Jupiter system at 10 pc in $\sim$20 min of integration. It would also be able to detect an Earth in a sun-Earth system at 6 pc in $\sim$1.5 hrs. There are $\sim$100 stars within 6 pc, and $\sim$450 stars within 10 pc of the sun.

3.6 *The Far Future: Interferometry on the Moon*

Interest in using the Moon as a platform for astronomical instruments goes back quite a few years (27, 73, 101). In 1989, on the 20th anniversary of the first Apollo landing on the Moon, NASA was asked to plan a return to the Moon and then a mission to Mars. Because of the availability of long baselines, the cold lunar night, the stable lunar soil, and the accurately known lunar orbit (168), the Moon was seen as a natural site for a long-baseline optical interferometer. Several NASA-sponsored workshops held in 1990 (26, 111) addressed lunar optical interferometry among other topics. The Bahcall report (112) also contained a chapter on lunar astronomy, and ESA held a series of workshops that led to a report on lunar optical interferometry (94).

The Moon has both the advantages of space—lack of an atmosphere—as well as the advantages of the Earth—a large, stable platform. At night the temperature drops to 100 K, making possible low temperature telescopes for infrared observations. A lot of real estate is available, and baselines as long as 10 km are feasible. In addition, its orbit is stable and known to very high accuracy so that sub-microarcsec astrometry is possible. The combination of very high angular resolution (10 μas with high sensitivity) and high astrometric accuracy (0.1 μas) would revolutionize almost every area of UV/optical/infrared astrophysics. A number of instrument concepts have been proposed to exploit these characteristics, including (24, 25, 85) and those in Table 2.

One instrument concept originally envisioned for a lunar interferometer is the starlight nulling interferometer, using a single-mode fiber for very high dynamic range imaging, discussed above. The goal was to null out the starlight so that the thermal radiation from an Earth-like planet at a distance of ~ 10 pc could be detected; at 10 μm, the Earth/Sun ratio is much more favorable than in the visible (1, 21). If the light from the central star were not present, an Earth-sized object would be easily detected with a 4 m telescope cooled below 70 K. An interferometer was needed for two reasons: It provided a mechanism for starlight cancellation, but more important, a long baseline was needed to resolve the star from the Earth-like planet. An Earth-sun system at 10 pc would be separated by 0.1″. An interferometer with an 80 m baseline would have a resolution of 0.025″ at 10 μm, separating those two objects by 4 pixels. A lunar optical interferometer with 50 m^2 of total collecting area and a maximum 2 km baseline would be able to image the infrared radiation from an Earth-like planet or planets, if they exist, around any of the nearest several thousand stars.

While at the end of 1991, interferometry on the Moon seems as far away as it did in early 1989, the discussion and activity in the field led to several interesting new concepts in instrumentation that will probably find their way into nearer-term interferometer projects. This activity naturally removed limitations in thinking about what is possible and what is not possible. Some of the ideas that came about as a result of thinking about what is possible on the Moon will turn out to be feasible on the Earth.

4. SUMMARY

Long-baseline interferometry began at the beginning of this century when Michelson performed his experiments on Mt. Wilson. In the decades following Michelson's pioneering work, optical interferometry gained a reputation as a field that was more technologically challenging than scientifically productive. In the 1980s that reputation began to fade as long-baseline interferometers were built in which finding the fringe was not a major technical triumph, but rather a routine event that happened many times each night. In the 1990s, interferometry takes another turn. The two largest telescope projects, the Keck observatory and ESO's VLT, both plan to have interferometric observational capabilities. These plans are in addition to a number of new long-baseline observatories proposed or under construction.

In the 1990s we expect interferometry to expand in a number of directions. The first is the use of three elements for closure-phase measurements, and then more elements for aperture-synthesis imaging. A second is a shift to the infrared. With the advent of the giant 8–10 m telescopes, the

combination of adaptive optics, large apertures, and long baselines will offer unprecedented sensitivity and angular resolution simultaneously. A third will be a shift in emphasis from building interferometers to building instruments for interferometers. Even during the 1980s, the technical problems of phasing two telescopes separated by 10's of meters taxed the technical ingenuity and budgets of those building the instruments. As these technologies mature, attentions and budgets will be directed at building various types of imaging spectrometers that will to some extent combine spectroscopic capability with high angular resolution. Perhaps most important of all, we will see in the 1990s a shift in the users of long-baseline interferometers, away from the builders of the instruments, to the general astronomy community. Space interferometry, while further in the future, will show the full advantages of long-baseline interferometry, initially with astrometry at microarcsec levels, and eventually with high resolution images of the central engines of AGNs and perhaps of Earth-like planets around nearby stars.

Acknowledgments

This review was prepared at the Jet Propulsion Laboratory, California Institute of Technology, under a contract with the National Aeronautics and Space Administration.

Literature Cited

1. Angel, J. R. P. 1989. See Ref. 10 ,pp. 81–95
2. Angel, J. R. P., Cheng, A. Y. S., Woolf, N. J. 1986. *Nature* 232: 341–43
3. Atherton, P. D., Greenaway, A. H., Noordam, J. E. 1985. See Ref. 93 , pp. 141–44
4. Beckers, J. M. 1990. *Proc. SPIE* 1236: 364–71
5. Beckers, J. M. 1990. *Proc. SPIE* 1236: 379–89
6. Beckers, J. M. 1990. *Proc. SPIE* 1236: 154–63
7. Beckers, J. M. 1991. *J. Optics (Paris)* 22: 73–83
8. Beckers, J. M., Enard, D., Faucherre, M., Merkle, F., di Benedetto, G. P., et al. 1990. *Proc. SPIE* 1236: 108–24
9. Beckers, J. M., Goad, L. E. 1987. In *Instrumentation for Ground-Based Optical Astronomy*, ed. L. Robinson, pp. 315–36. New York: Springer-Verlag
9a. Beckers, J. M., Merkle, F., eds. 1992.*High-Resolution Imaging by Interferometry II* Conf. and Workshop Proc. ESO. In press
10. Bely, P. Y., Burrows, C. J., Illingworth, G. D., eds. 1989. *The Next Generation Space Telescope*. Baltimore, MD: Space Telesc. Sci. Inst.
11. Bely, P. Y., Burrows, C. J., Roddier, F. 1990. See Ref. 22 , pp. 198–205
12. Bely, P. Y., Burrows, C. J., Roddier, F., Weigelt, G. 1989. *Proc. SPIE* 1130: 92–100
13. Bely, P. Y., Burrows, C. J., Roddier, F., Weigelt, G. 1991. See Ref. 152 , pp. 81–89
14. Bender, P. L., Stebbins, R. T. 1991. See Ref. 152 , pp. 101–6
15. Bester, M., Danchi, W. C., Degiacomi, C. G., Greenhill, L. J., Townes, C. H. 1991. *Bull. Am. Astron. Soc.* 23: 894 (Abstr.)
16. Bester, M., Danchi, W. C., Degiacomi, C. G., Townes, C. H., Geballe, T. R. 1991. *Ap. J. Lett.* 367: L27–L31
17. Bester, M., Danchi, W. C., Townes, C. H. 1990. See Ref. 22 , pp. 40–48

18. Born, M., Wolf, E. 1980. *Principles of Optics*. Oxford: Pergamon. 6th ed.
19. Boyce, P. B., Reasenberg, R. D., eds. 1984. *Workshop on High Angular Resolution Optical Interferometry*. Bull. Am. Astron. Soc., vol. 16, pp. 747–837
20. Bracewell, R. N. 1978. *Nature* 274: 780–81
21. Bracewell, R. N., MacPhie, R. H. 1979. *Icarus* 38: 136–47
22. Breckinridge, J. B., ed. 1990. *Amplitude and Intensity Spatial Interferometry*, Proc. SPIE 1237. Bellingham, WA: SPIE
23. Brown, R. A. 1990. See Ref. 111 , pp. 87–94
24. Burke, B. F. 1986. See Ref. 27, pp. 73–83
25. Burns, J. O. 1991. See Ref. 152 , pp. 107–16
26. Burns, J. O., Johnson, S. W., Duric, N., eds. 1992. *Proceedings of the Workshop on a Lunar Optical-UV-IR Synthesis Array (LOUISA)*. NASA Conf. Publ. In press
27. Burns, J. O., Mendell, W. W., eds. 1988. *Future Astronomical Observatories on the Moon*. NASA Conf. Publ. 2489
28. Carleton, N. P. 1988. See Ref. 102 , pp. 939–48
29. Colavita, M. M. 1991. See Ref. 152 , pp. 125–34
30. Colavita, M. M., Shao, M. 1988. See Ref. 102 , pp. 833–40
31. Colavita, M. M., Shao, M., Hines, B. E., Levine, B. M., Gershman, R. 1991. *Proc. SPIE* 1494: 168–81
32. Colavita, M. M., Shao, M., Staelin, D. H. 1987. *Appl. Opt.* 26: 4106–12
33. Colavita, M. M., Shao, M., Staelin, D. H. 1987. *Appl. Opt.* 26: 4113–22
34. Connes, P., Froehly, C., Facq, P. 1985. See Ref. 93 , pp. 49–62
35. Connes, P., Michel, G. 1975. *Appl. Opt.* 14: 2067–84
36. Dainty, J. C. 1984. In *Laser Speckle and Related Phenomena*, ed. J. C. Dainty, pp. 257–320. Berlin: Springer-Verlag
37. Danchi, W. C., Bester, M., Degiacomi, C. G., McCullough, P. R., Townes, C. H. 1990. *Ap. J. Lett.* 359: L59–L63
38. Danchi, W. C., Bester, M., Townes, C. H. 1988. See Ref. 102, pp. 867–76
39. Davis, J. 1988. See Ref. 102 , pp. 817–21
40. Davis, J., Tango, W. J. 1985. *Proc. Astron. Soc. Aust.* 6: 38–43
41. Davis, J., Tango, W. J. 1985. *Proc. Astron. Soc. Aust.* 6: 34–38
42. Davis, J., Tango, W. J. 1986. *Nature* 323: 234–35
43. di Benedetto, G. P., Rabbia, Y. 1987. *Astron. Astrophys.* 188: 114–24
44. Dyck, H. M., Benson, J. A. 1988. See Ref. 102 , pp. 1015–20
45. Dyck, H. M., Benson, J. A., Mason, W. L., Ridgway, S. T., Howell, R. R. 1990. See Ref. 22 , pp. 31–39
46. Deleted in proof
47. Faucherre, M., Delabre, B., Diericks, P., Merkle, F. 1990. See Ref. 22 , pp. 206–17
48. Faucherre, M., Greenaway, A. H., Merkle, F., Noordam, J. E., Perryman, M. A. C., et al. 1989. *Proc. SPIE* 1130: 101–8
49. Faucherre, M., Greenaway, A. H., Merkle, F., Noordam, J. E., Perryman, M. A. C., et al. 1989. In *Diffraction-Limited Imaging with Very Large Telescopes*, ed. D. Alloin, J. M. Mariotti, pp. 389–404. Dordrecht: Kluwer
50. Fizeau, A. H. 1868. *C. R. Acad. Sci. (Paris)* 66: 934
51. Foy, R., Labeyrie, A. 1985. *Astron. Astrophys.* 152: L29–L31
52. Fried, D. L. 1965. *J. Opt. Soc. Am.* 55: 1427–35
53. Fried, D. L. 1966. *J. Opt. Soc. Am.* 56: 1380–84
54. Fugate, R. Q., Fried, D. L., Ameer, G. A., Boeke, B. R., Brown, S. L., et al. 1991. *Nature* 353: 144–46
55. Gardner, C. S., Welsh, B. M., Thompson, L. A. 1990. *Proc. IEEE* 78: 1721–43
56. Gay, J., Mekarnia, D. 1988. See Ref. 102 , pp. 811–16
57. Geldzahler, B., ed. 1989. *Proceedings of the Workshop on Technologies for Space Optical Interferometry*. NASA
58. Gershman, R., Mahoney, M. J., Rayman, M. D., Shao, M., Snyder, G. C. 1991. *Proc. SPIE* 1494: 160–67
59. Gezari, D. Y., Roddier, F., Roddier, C. 1990. *Spatial Interferometry in Optical Astronomy*. Ref. Publ. 1245, NASA
60. Granes, P., Vakili, F., Thom, C. 1986. *Astron. Astrophys.* 165: L13–L15
61. Greenwood, D. P. 1977. *J. Opt. Soc. Am.* 67: 390–93
62. Hanbury Brown, R. 1974. *The Intensity Interferometer*. London: Taylor & Francis
63. Hanbury Brown, R., Davis, R. J., Allen, L. R. 1967. *MNRAS* 137: 375–92
64. Hanbury Brown, R., Davis, R. J., Allen, L. R. 1974. *MNRAS* 167: 121–36
65. Hanbury Brown, R., Twiss, R. Q. 1956. *Nature* 178: 1046–48
66. Haniff, C. A., Mackay, C. D., Titterington, D. J., Sivia, D., Baldwin, J. E., et al 1987. *Nature* 328: 694–96

67. Hardy, J. W. 1978. *Proc. IEEE* 66: 651–97
68. Hughes, J. A., Hutter, D. J. 1990. See Ref. 22 , pp. 296–300
69. Hughes, J. A., Hutter, D. J. 1990. See Ref. 22 , pp. 10–21
70. Hutter, D. J., Johnston, K. J., Mozurkewich, D., Simon, R. S., Colavita, M. M., et al. 1989. *Ap. J.* 340: 1103–11
71. Ishimaru, A. 1978. *Wave Propagation and Scattering in Random Media.* New York: Academic
72. Johnson, M. A., Betz, A. L., Townes, C. H. 1974. *Phys. Rev. Lett.* 33: 1617–20
73. Johnson, S. W. 1991. See Ref. 26
74. Jones, D. L. 1991. See Ref. 152 , pp. 117–24
75. Koechlin, L. 1988. See Ref. 102 , pp. 695–704
76. Koechlin, L., Bonneau, D., Vakili, F. 1979. *Astron. Astrophys.* 80: L13–L14
77. Koechlin, L., Rabbia, Y. 1985. *Astron. Astrophys.* 153: 91–98
78. Korff, D., Dryden, G., Leavitt, R. P. 1975. *J. Opt. Soc. Am.* 65: 1321–28
79. Kovalevsky, J. 1984. *Space Sci. Rev.* 39: 1–63
80. Kulkarni, S. R., Prasad, S., Nakajima, T. 1991. *J. Opt. Soc. Am. A* 8: 499–510
81. Labeyrie, A. 1970. *Astron. Astrophys.* 6: 85–87
82. Labeyrie, A. 1975. *Ap. J.* 196: L71–L75
83. Labeyrie, A., Authier, B., Boit, J. L., de Graauw, T., Kibblewhite, E., et al. 1984. *Bull. Am. Astron. Soc.* 16: 828–31
84. Labeyrie, A., Authier, B., de Graauw, T., Kibblewhite, E., Weigelt, G. 1985. See Ref. 93 , pp. 27–34
85. Labeyrie, A., Mourard, D. 1990. See Ref. 111 , pp. 538–49
86. Labeyrie, A., Schumacher, G., Dugue, M., Thom, C., Bourlon, P., et al. 1986. *Astron. Astrophys.* 162: 359–64
87. Lacasse, M. G., Traub, W. A. 1985. See Ref. 93 , pp. 133–40
88. Laskin, R. A., Redding, D. C., Breckenridge, W. G., Shao, M. 1990. In *AAS Rocky Mountain Guidance and Control Conf.* Am. Astronaut. Soc.
89. Lawrence, R. S., Strohbehn, J. W. 1970. *Proc. IEEE* 58: 1523–45
90. Layman, W. E. 1989. See Ref. 10 , pp. 263–69
91. Lindegren, L. 1980. *Astron. Astrophys.* 89: 41–47
92. Longdon, N., David, V., eds. 1987. *Workshop on Optical Interferometry in Space* SP–273. Noordwijk: ESA
93. Longdon, N., Melita, O., eds. 1985. *Colloquium on Kilometric Optical Arrays in Space* SP–226. Noordwijk: ESA
94. Lunar Interferometry Study Team. 1992. *Lunar Interferometry: An Interim Report to the Space Science Advisory Committee.* Tech. Rep. Noordwijk: ESA. In press
95. Mackay, C. D., Baldwin, J. E. 1988. See Ref. 102 , pp. 935–38
96. Mariotti, J. M., Ridgway, S. T. 1988. *Astron. Astrophys.* 195: 350–63
97. McAlister, H. A. 1988. See Ref. 102 , pp. 971–79
98. McAlister, H. A. 1988. See Ref. 102 , pp.3–18
99. McAlister, H. A., Bagnuolo, W. B. Jr., Hartkopf, W. J. 1990. See Ref. 22 , pp. 22–30
100. Meinel, A. B., Meinel, M. P., Breckinridge, J. B. 1992. See Ref. 9a
101. Mendell, W. W., ed. 1988. *Lunar Bases and Space Activities in the 21st Century* Houston: Lunar Planetary Inst.
102. Merkle, F., ed. 1988. *High-Resolution Imaging by Interferometry.* Conf. & Workshop Proc. vol. 29. ESO
103. Merkle, F. 1988. *J. Opt. Soc. Am. A* 5: 904–13
104. Michelson, A. A. 1920. *Ap. J.* 51: 257–62
105. Michelson, A. A., Pease, F. G. 1921. *Astrophys J.* 53: 249–59
106. Mourard, D. 1988. See Ref. 102 , pp. 729–34
107. Mozurkewich, D., Hutter, D. J., Johnston, K. J., Simon, R. S., Shao, M., et al. 1988. *Astron. J.* 95: 1269–77
108. Mozurkewich, D., Johnston, K. J., Simon, R. S. 1990. See Ref. 22 , pp. 120–27
109. Mozurkewich, D., Johnston, K. J., Simon, R. S., Bowers, P. F., Gaume, R., et al. 1991. *Astron. J.* 101: 2207–19
110. Mozurkewich, D., Johnston, K. J., Simon, R. S., Hutter, D. J., Colavita, M. M., et al. 1988. See Ref. 102 , pp. 851–54
111. Mumma, M. J., Smith, H. J., eds. 1990. *Astrophysics from the Moon* Conf. Proc. 207. AIP
112. National Research Council. 1991. *The Decade of Discovery in Astronomy and Astrophysics.* Wash., DC: Natl. Acad.
113. Noordam, J. E., Atherton, P. D., Greenaway, A. H. 1985. See Ref. 93 , pp. 63–69
114. Noordam, J. E., Bely, P. Y., Faucherre, M., Greenaway, A. H., Merkle, F., et al. 1990. *A Proposed Medium-Term Strategy for Optical Interferometry in Space.* Tech. Rep. Noordwijk: ESA
115. Noordam, J. E., Greenaway, A. H.,

Bregman, J. D., le Poole, R. S. 1987. See Ref. 92, pp. 51–59
116. Pan, X. P., Shao, M., Colavita, M. M., Armstrong, J. T., Mozurkewich, D., et al. 1990. See Ref. 22 , pp. 301–15
117. Pan, X. P., Shao, M., Colavita, M. M., Armstrong, J. T., Mozurkewich, D., et al. 1992. *Ap. J.* 384: 624–33
118. Pan, X. P., Shao, M., Colavita, M. M., Mozurkewich, D., Simon, R. S., et al. 1990. *Ap. J.* 356: 641–45
119. Pearson, T. J., Readhead, A. C. S. 1984. *Annu. Rev. Astron. Astrophys.* 22: 97–130
120. Pease, F. G. 1930. *Sci. Am.* 143: 290–94
121. Pease, F. G. 1931. *Ergeb. Exakten Naturwiss.* 10: 84–96
122. Prasad, S., Kulkarni, S. R. 1989. *J. Opt. Soc. Am. A* 6: 1702–14
123. Primmerman, C. A., Murphy, D. V., Page, D. A., Zollars, B. G., Barclay, H. T. 1991. *Nature* 353: 141–43
124. Reasenberg, R. D. 1984. *Bull. Am. Astron. Soc.* 16: 758–66
125. Reasenberg, R. D. 1990. See Ref. 22 , pp. 128–37
126. Reasenberg, R. D. 1991. See Ref. 152 , pp. 51–65
127. Reasenberg, R. D., Babcock, R. W., Chandler, J. F., Gorenstein, M. V., Huchra, J. P., et al. 1988. *Astron. J.* 32: 1731–45
128. Reinheimer, T., Weigelt, G. 1987. *Astron. Astrophys.* 176: L17–L20
129. Rigaut, F., Rousset, G., Kern, P., Fontanella, J. C., Gaffard, J. P., et al 1991. *Astron. Astrophys.* 250: 280–90
130. Roddier, F. 1981. In *Progress in Optics XIX*, ed. E. Wolf, pp. 281–376. Amsterdam: North-Holland
131. Roddier, F. 1986. *Opt. Commun.* 60: 145–48
132. Roddier, F. 1988. See Ref. 102 , pp. 565–74
133. Roddier, F., Gilli, J. M., Vernin, J. 1982. *J. Optics (Paris)* 13: 63–70
134. Roddier, F., Léna, P. 1984. *J. Optics (Paris)* 15: 171–82
135. Roddier, F., Léna, P. 1984. *J. Optics (Paris)* 15: 363–74
136. Rogstad, D. H. 1968. *Appl. Opt.* 7: 585–88
137. Rousset, G., Fontanella, J. C., Kern, P., Gigan, P., Rigaut, F., et al. 1990. *Astron. Astrophys.* 230: L29–L32
138. Schumacher, G., Boischot, A., Cruzalebes, P., Dugue, M., Koechlin, L., et al. 1988. See Ref. 102 , pp. 743–56
139. Shaklan, S. 1990. *Opt. Eng.* 29: 684–89
140. Shaklan, S. B., Shao, M., Colavita, M. M. 1992. See Ref. 9a
141. Shao, M. 1989. See Ref. 10 , pp. 160–68
142. Shao, M. 1990. See Ref. 111 , pp. 486–94
143. Shao, M. 1991. See Ref. 152 , pp. 23–32
144. Shao, M. 1991. *Proc. SPIE* 1494: 347–56
145. Shao, M. 1991. See Ref. 152 , pp. 67–73
146. Deleted in proof
147. Shao, M., Colavita, M. M., Hines, B. E., Hershey, J. L., Hughes, J. A., et al. 1990. *Astron. J.* 100: 1701–11
148. Shao, M., Colavita, M. M., Hines, B. E., Pan, X., Mozurkewich, D., et al. 1991. *Bull. Am. Astron. Soc.* 23: 830(Abstr.)
149. Shao, M., Colavita, M. M., Hines, B. E., Staelin, D. H., Hutter, D. J., et al. 1988. *Ap. J.* 327: 905–10
150. Shao, M., Colavita, M. M., Hines, B. E., Staelin, D. H., Hutter, D. J., et al. 1988. *Astron. Astrophys.* 193: 357–71
151. Shao, M., Colavita, M. M., Staelin, D. H., Johnston, K. J., Simon, R. S., et al. 1987. *Astron J.* 93: 1280–86
152. Shao, M., Kulkarni, S., Jones, D., eds. 1991. *Workshop Proceedings: Science Objectives and Architectures for Optical Interferometry in Space*, JPL Int. Doc. D–8540, vol. 1. Pasadena, CA: JPL
153. Shao, M., Staelin, D. H. 1977. *J. Opt. Soc. Am.* 67: 81–86
154. Shao, M., Staelin, D. H. 1980. *Appl. Opt.* 19: 1519–22
155. Stachnik, R. V., Faucherre, M. 1987. See Ref. 92 , pp. 61–62
156. Stachnik, R. V., Gezari, D. Y. 1985. See Ref. 93 , pp. 35–42
157. Stebbins, R. T., Bender, P. L., Faller, J. E. 1987. See Ref. 92 , pp. 85–89
158. Strandberg, M. W. P. 1957. *Phys. Rev.* 106: 617–20
159. Strohbehn, J. W., ed. 1978. *Laser Beam Propagation in the Atmosphere*. Berlin: Springer-Verlag
160. Sutton, E. C., Betz, A. L., Storey, J. W. V., Spears, D. L. 1979. *Ap. J.* 230: L105–8
161. Sutton, E. C., Storey, J. W. V., Betz, A. L., Townes, C. H., Spears, D. L. 1977. *Ap. J.* 217: L97–L100
162. Sutton, E. C., Storey, J. W. V., Townes, C. H., Spears, D. L. 1978. *Ap. J.* 224: L123–26
163. Sutton, E. C., Subramanian, S., Townes, C. H. 1982. *Astron. Astrophys.* 110: 324–31
164. Synnott, S. P. 1991. See Ref. 152 , pp. 91–100
165. Synnott, S. P. 1991. *Proc. SPIE* 1494: 334–43

166. Tango, W. J., Twiss, R. Q. 1974. *Appl. Opt.* 13: 1814–19
167. Tango, W. J., Twiss, R. Q. 1980. In *Progress in Optics XVII*, ed. E. Wolf, pp. 241–77. Amsterdam: North-Holland
168. Taylor, G. J. 1991. See Ref. 26
169. Terrile, R. J., Ftaclas, C. 1989. See Ref. 10 , pp. 225–31
170. Thompson, A. R., Moran, J. M., Swenson, G. W. Jr. 1986. *Interferometry and Synthesis in Radio Astronomy*. New York: Wiley
171. Thompson, L. A., Gardner, C. S. 1987. *Nature* 328: 229–31
172. Townes, C. H. 1984. *J. Astrophys. Astron.* 5: 111–30
173. Traub, W. A. 1985. See Ref. 93 , pp. 43–48
174. Traub, W. A. 1987. See Ref. 92 , pp. 67–68
175. Traub, W. A. 1987. See Ref. 92 , pp. 63–66
176. Traub, W. A. 1991. See Ref. 152 , pp. 75–76
177. Traub, W. A. 1991. See Ref. 152 , pp. 77–79
178. Traub, W. A., Massa, D. L., Endal, A. S., Beckers, J. M., Latham, D. W., et al. 1987. *Proc. SPIE* 751: 72–82
179. Weaver, L. D., Fender, J. S., De Hainaut, C. R. 1988. *Opt. Eng.* 27: 730–35
180. Weigelt, G. 1977. *Opt. Comm.* 21: 55–59.